AD-A175 824 THERMOVISCOELASTIC CHARACTERIZATION AND ANALYSIS OF FIBER COMPOSITE SPACE (U) MATERIALS SCIENCES CORP SPRING HOUSE PA B J SULLIVAN ET AL FEB 86 1/1

UNCLASSIFIED MSC-TFR-1614/1505 AFOSR-TR-86-2111 F/G 11/4 NL

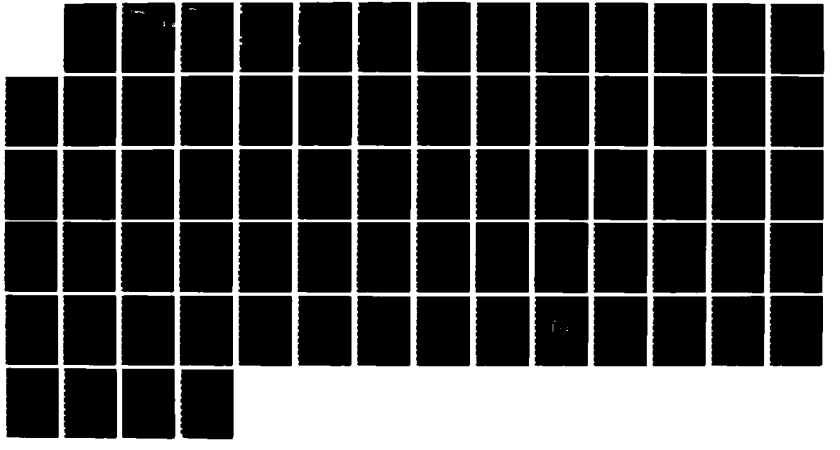

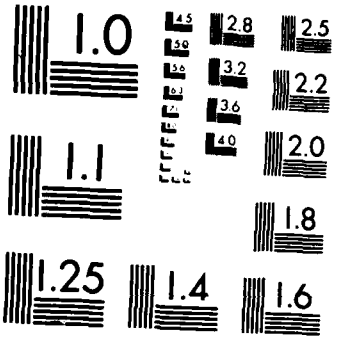

(2)

Materials Sciences Corporation

THERMOVISCOELASTIC CHARACTERIZATION AND ANALYSIS OF FIBER COMPOSITE SPACE STRUCTURES

B. J. Sullivan, E. A. Humphreys, and
Zvi Hashin

"The views and conclusions contained in this document are those of the authors and should not be interpreted as necessarily representing the official policies or endorsements, either expressed or implied, of the Air Force Office of Scientific Research of the U.S. Government."

Air Force Office of Scientific Research
Bolling Air Force Base, DC

MSC TFR 1614/1505
February, 1986

THERMOVISCOELASTIC CHARACTERIZATION AND ANALYSIS OF FIBER COMPOSITE SPACE STRUCTURES

Technical Final Report
MSC TFR 1614/1505
February, 1986

Prepared for:
Air Force Office of Scientific Research
Building 410
Bolling AFB, Washington, D.C. 20332

Gwynedd Plaza II, Bethlehem Pike, Spring House, PA 19477 • 215-542-8400

REPORT DOCUMENTATION PAGE

READ INSTRUCTIONS BEFORE COMPLETING FORM

1. REPORT NUMBER: AFOSR-TR- 86-2111
2. GOVT ACCESSION NO.
3. RECIPIENT'S CATALOG NUMBER

4. TITLE (and Subtitle): Thermoviscoelastic Characterization and Analysis of Fiber Composite Space Structures

5. TYPE OF REPORT & PERIOD COVERED: Final Report 10/1/84 - 12/31/85

6. PERFORMING ORG. REPORT NUMBER

7. AUTHOR(s): B. J. Sullivan, E. A. Humphreys, and Zvi Hashin

8. CONTRACT OR GRANT NUMBER(s): F49620-85-C-0004

9. PERFORMING ORGANIZATION NAME AND ADDRESS: Materials Sciences Corporation, Gwynedd Plaza II, Bethlehem Pike, Spring House, PA 19477

10. PROGRAM ELEMENT, PROJECT, TASK AREA & WORK UNIT NUMBERS: 61102F 2302/B1

11. CONTROLLING OFFICE NAME AND ADDRESS: Air Force Office of Scientific Research, Building 410, Bolling AFB, Washington, D.C. 20332

12. REPORT DATE: February 1986

13. NUMBER OF PAGES: NA

14. MONITORING AGENCY NAME & ADDRESS (if different from Controlling Office): same as 11

15. SECURITY CLASS. (of this report): Unclassified

15a. DECLASSIFICATION/DOWNGRADING SCHEDULE

16. DISTRIBUTION STATEMENT (of this Report)

Approved for public release; distribution unlimited

17. DISTRIBUTION STATEMENT (of the abstract entered in Block 20, if different from Report)

18. SUPPLEMENTARY NOTES

19. KEY WORDS (Continue on reverse side if necessary and identify by block number)

Carbon/Epoxy Composites
Thermoviscoelasticity
Effective Constitutive Equations
Dynamic Analysis
Complex Compliances
Composite Structures
Eigensolutions

20. ABSTRACT (Continue on reverse side if necessary and identify by block number)

This report begins with the development of the time and temperature-dependent effective constitutive equations for unidirectional fiber composites. The fibers were represented as transversely isotropic and linearly elastic, temperature dependent elements. The deviatoric components of the isotropic matrix material were treated as linearly viscoelastic and thermorheologically complex, while the dilatation components

20. Abstract

were represented as elastic and temperature dependent. Numerical simulations of a series of isothermal creep tests were performed to determine th effective creep compliance parameters of the composite constitutive equations. The macromechanical response of a composite structural element, as predicted by the effective constitutive equations and their derived parameters, was then verified using results computed using a micromechanical model which explicitly included the fiber and matrix as discrete phases. To determine the potential existence and form of a composite complex modulus, the response of unidirectional composite structural elements to simultaneous sinusoidal temperature and mechanical loads was investigated. Finally, solutions of free vibration and transient dynamic analyses of some simple composite structures were performed to examine the effects of the thermoviscoelastic behavior on the damped response of some simple composite structures.

PREFACE

This report summarizes the results of a study performed under Air Force Office of Scientific Research Contract F49620-85-C-0004 during the period October 1, 1984 to December 31, 1985. The principal investigators for Materials Sciences Corporation (MSC) are Dr. Brian J. Sullivan and E. A. Humphreys. Dr. Zvi Hashin, Scientific Advisor, also contributed to this report. The technical monitor for the Air Force Office of Scientific Research is Dr. Anthony Amos.

APPROVED BY:

B. Walter Rosen
Program Manager

TABLE OF CONTENTS

		Page
1.	INTRODUCTION	1
2.	THERMOVISCOELASTIC CONSTITUTIVE RELATIONS	2
	2.1. DEVELOPMENT OF EFFECTIVE THERMOVISCOELASTIC EQUATIONS	2
	2.2. LITERATURE SURVEY OF THERMOVISCOELASTIC MATERIAL PROPERTIES	18
	2.3. EVALUATION OF EFFECTIVE THERMOVISCOELASTIC PARAMETERS	18
	2.4. VERIFICATION OF EFFECTIVE COMPOSITE CONSTITUTIVE EQUATIONS	19
3.	RESPONSE TO SINUSOIDAL TEMPERATURE AND LOAD	21
4.	DYNAMIC ANALYSES OF THERMOVISCOELASTIC COMPOSITE STRUCTURES	22
	4.1. INTRODUCTION	22
	4.2. FREE FLEXURAL VIBRATIONS OF CANTILEVERED UNIDIRECTIONAL BEAM	22
	4.3. EFFECT OF TRANSIENT LOADS AND TEMPERATURES ON A SIMPLE COMPOSITE STRUCTURE	28
5.	DISCUSSION AND RECOMMENDATIONS	31
REFERENCES		32
TABLE		35
FIGURES		36

1. INTRODUCTION

This report summarizes the work associated with the evaluation of the time and temperature-dependent response of unidirectional fiber reinforced composite structures and structural elements. An examination of this response is of fundamental importance in understanding the behavior of fiber composite structures subjected to an environment which includes severe temperature variations. The proposed large orbiting space structures, e.g. solar electric power stations, communication satellites with large antennae, etc., are examples of structures which will undergo severe temperature cycling. Thus, the utilization of graphite/polymer composites in these designs requires that the thermo-mechanical response of structural elements composed of such materials be investigated.

The carbon fiber/polymeric matrix composites are known to exhibit time dependent, or viscoelastic behavior. In addition, the time dependent characteristics are modified by the temperature environment experienced by the material, so that a thermoviscoelastic representation must be used. In particular, a thermorheologically complex material (TCM) model of the matrix, and thus the unidirectional fiber composite, has been employed here.

The objectives of the current efforts in the thermoviscoelastic analysis of fiber reinforced composite structures were threefold. Initially, attention was focused at developing the form and parameters of the thermorheologically complex constitutive relations for unidirectional fiber composites of the polymeric matrix type. Following the successful characterization of the effective constitutive relations, the response of unidirectional TCM composite structural elements to simultaneous sinusoidal temperature and mechanical loads was determined, in order to investigate the existence of complex moduli/compliances in this situation. Finally, temperature-dependent eigensolutions, and dynamic analyses of transient load and temperature conditions, on some simple composite structures were performed, with the purpose of investigating the extent and sources of damped response in the TCM composite structures.

2. THERMOVISCOELASTIC CONSTITUTIVE RELATIONS

2.1. DEVELOPMENT OF EFFECTIVE THERMOVISCOELASTIC EQUATIONS

The effective constitutive equations for unidirectional composites are dependent on the mechanical behavior of the individual composite constituents. In this work, the fibers were represented as transversely isotropic and linearly elastic, temperature dependent elements. The matrix material surrounding the fibers was taken as isotropic. The deviatoric or shear components of the matrix response were assumed to be linear viscoelastic and thermorheologically complex. The dilational components have been considered to be elastic and temperature dependent. Note that this characterization of matrix behavior as elastic in dilatation and viscoelastic in shear is consistent with the typically assumed response in three-dimensional viscoelastic stress analysis [1].

The development of the effective constitutive equations was performed by assuming that the form of the composite stress-strain equations in all deformation modes (dilational and deviatoric) was identical to the form of the matrix constitutive equation in shear. For typical fiber volume fractions, this is a reasonable assumption. The most simple form of a thermorheologically complex viscoelastic stress-strain equation was used; this is one which includes a horizontal shift, representing time-temperature equivalence, and a single vertical shift for modeling the temperature dependence of the initial modulus. This is a slight variation of the thermorheologically complex equation proposed by Schapery [2].

The form of the thermorheologically complex viscoelastic material model representing the matrix material in shear is given by the symbolic equation:

$$2e_{ij} = g \otimes s_{ij} \tag{2.1.1}$$

which represents the more complete form

$$2e_{ij}(t) = g(0)V(\phi)\, s_{ij}(t) + \Delta g(\xi)\, s_{ij}(0) + \int_{0+}^{t} \Delta g(\xi-\xi') \frac{\partial s_{ij}(t')}{\partial t'} dt' \tag{2.1.2}$$

where

e_{ij}, s_{ij} = the deviatoric strain and stress respectively,

$g(0)$ = the instantaneous shear creep compliance,

$g(\xi)$ = the time dependent shear creep compliance,

$V(\phi)$ = a vertical shift factor, and

$\phi(t)$ = temperature.

Also, the parameter ξ represents the reduced time and is given by the equation

$$\xi(t) = \int_0^t h[\phi(u)]du \qquad (2.1.3)$$

where

$h(\phi)$ = a horizontal shift factor.

Note that the temperature dependence of the stress-strain equation is represented by the horizontal and vertical shift factors. The reduced time allows the viscoelastic response at any temperature to be obtained from a master response at reference temperature through a horizontal shift along the time axis. The role of the vertical shift factor is to model the temperature dependence of the initial compliance. Note that in isothermal, temperature independent viscoelasticity, both the horizontal and vertical shift factors are unity. Further background into the development of the TCM constitutive equations may be found in Schapery [2].

With respect to the thermoviscoelastic unidirectional fiber composite, since the matrix material is transversely isotropic, and because of the random nature of fiber placement, the composite is statistically transversely isotropic. Its effective thermoviscoelastic constitutive

relations may be written using the simplified notation of equation (2.1.1) as

$$\bar{\epsilon}_{11} = S_{11}^* \otimes \bar{\sigma}_{11} + S_{12}^* \otimes \bar{\sigma}_{22} + \bar{S}_{12}^* \otimes \bar{\sigma}_{33} + \alpha_L^* \otimes \phi$$

$$\bar{\epsilon}_{22} = S_{12}^* \otimes \bar{\sigma}_{11} + S_{22}^* \otimes \bar{\sigma}_{22} + S_{23}^* \otimes \bar{\sigma}_{33} + \alpha_T^* \otimes \phi$$

$$\bar{\epsilon}_{33} = S_{12}^* \otimes \bar{\sigma}_{11} + S_{23}^* \otimes \bar{\sigma}_{22} + S_{22}^* \otimes \bar{\sigma}_{33} + \alpha_T^* \otimes \phi \qquad (2.1.4)$$

$$2\bar{\epsilon}_{12} = S_{44}^* \otimes \bar{\sigma}_{12}$$

$$2\bar{\epsilon}_{13} = S_{44}^* \otimes \bar{\sigma}_{13}$$

$$2\bar{\epsilon}_{23} = S_{55}^* \otimes \bar{\sigma}_{23}$$

Where

S_{ij}^* - the effective creep compliances, and

α_L^*, α_T^* - the effective compliances for the longitudinal and transverse coefficients of thermal expansion.

Note that the bars over the strains and stresses indicate average strains and stresses in the composite.

The complete set of effective creep compliance parameters include

$S_{ij}^{*}(0)$ - the effective instantaneous creep compliances,

$\Delta S_{ij}^{*}(t)$ - the effective time dependent creep compliances,

$h_{ij}^{*}(\phi)$ - the effective horizontal shifts, and

$V_{ij}^{*}(\phi)$ - the effective vertical shifts.

Thus, unlike the case with elastic materials in which effective moduli or compliances are determined from the constant response to a constant mechanical or thermal input, a series of isothermal creep tests must be performed in each mode of deformation, to determine the time and temperature dependence for the entire set of effective creep compliances of the composite constitutive equations.

Consider first the case of longitudinal shear. The effective stress-strain equation is given by

$$2\bar{\epsilon}_{12}(t) = S_{44}^{*}(0)\, V_{44}^{*}(\phi)\bar{\sigma}_{12}(t) + \Delta S_{44}^{*}(\xi)\bar{\sigma}_{12}(0) \qquad (2.1.5)$$

$$+ \int_{0^{+}}^{t} \Delta S_{44}^{*}(\xi-\xi')\frac{d\bar{\sigma}_{12}(t')}{dt'}\, dt'$$

where

$$\xi = \xi(u) = \int_{-\infty}^{u} h_{44}^{*}[\phi(\tau)]d\tau \qquad (2.1.6)$$

Suppose we simulate an isothermal creep test in which

$$\bar{\sigma}_{12}(t) = H(t)\sigma_\circ$$

$$\phi(t) = H(t)\phi_\circ \tag{2.1.7}$$

where H(t) is the heavy-side (unit) step function defined such that

$$H(t) = \begin{cases} 0 & t < 0 \\ 1 & t \geq 0 \end{cases} \tag{2.1.8}$$

The stress-strain equation (2.1.5) gives

$$2\bar{\epsilon}_{12}(t) = S_{44}^*(0)V_{44}^*(\phi_\circ)\sigma_\circ + \Delta S_{44}^*(h_{44}^*(\phi_\circ)\cdot t)\sigma_\circ \tag{2.1.9}$$

The shift functions $h_{44}^*(\phi)$ and $V_{44}^*(\phi)$ are defined so that

$$h_{44}^*(\phi_R) = V_{44}^*(\phi_R) = 1 \tag{2.1.10}$$

where ϕ_R is the reference temperature. In this way, by performing the isothermal creep test at $\phi = \phi_R$ the creep function $S_{44}^*(t)$ is determined:

$$S_{44}^*(0) + \Delta S_{44}^*(t) = \frac{2\bar{\epsilon}_{12}(t,\phi_R)}{\sigma_\circ} \tag{2.1.11}$$

At t=0, $\Delta S_{44}^*(0) = 0$ by definition, so that

$$S_{44}^{*}(0) = \frac{2\bar{\epsilon}_{12}(0,\phi_R)}{\sigma_o} \qquad (2.1.12)$$

and for $t \neq 0$ we find

$$\Delta S_{44}^{*}(t) = \frac{2\bar{\epsilon}_{12}(t,\phi_R) - 2\bar{\epsilon}_{12}(0,\phi_R)}{\sigma_o} \qquad (2.1.13)$$

Now, the isothermal creep test at $\phi = \phi_o$ can be used to determine both $h_{44}^{*}(\phi)$ and $V_{44}^{*}(\phi)$ as follows. At $t = 0$ we get

$$V_{44}^{*}(\phi_o) = \frac{2\bar{\epsilon}_{12}(0,\phi_o)}{S_{44}^{*}(0)\cdot\sigma_o} \qquad (2.1.14)$$

which provides the vertical shift $V_{44}^{*}(\phi_o)$. This leaves the horizontal shift $h_{44}^{*}(\phi_o)$ as the only other unknown. At some other time during the creep test, e.g. $t = \hat{t}$, we get

$$\Delta S_{44}^{*}(h_{44}^{*}(\phi_o)\cdot\hat{t}) = \frac{2\bar{\epsilon}_{12}(\hat{t},\phi_o) - 2\bar{\epsilon}_{12}(0,\phi_o)}{\sigma_o} = \Delta S_{44}^{*}(\xi_{44}) \qquad (2.1.15)$$

from which

$$h_{44}^{*}(\phi_o) = \xi_{44}/\hat{t} \qquad (2.1.16)$$

Thus, by performing a series of isothermal creep tests at a range of temperatures, both $h_{44}^{*}(\phi)$ and $V_{44}^{*}(\phi)$ can then be determined.

Consider now the case of applied longitudinal stress coupled with a uniform temperature distribution, with all other stresses zero. Again simulating an isothermal creep test, we apply the loads

$$\bar{\sigma}_{11}(t) = H(t)\sigma_L$$

$$\phi(t) = H(t)\phi_o \tag{2.1.17}$$

in which case from the stress-strain relations (2.1.4) we have the two equations

$$\bar{\epsilon}_{11}(t,\phi_o) = S_{11}^*(0)V_{11}^*(\phi_o)\sigma_L + \Delta S_{11}^*(\xi)\sigma_L + \alpha_L^*(t,\phi_o)\cdot\phi_o \tag{2.1.18}$$

$$\bar{\epsilon}_{22}(t,\phi_o) = S_{12}^*(0)V_{12}^*(\phi_o)\sigma_L + \Delta S_{12}^*(\xi)\sigma_L + \alpha_L^*(t,\phi_o)\cdot\phi_o \tag{2.1.19}$$

Now define

$$\hat{\epsilon}_{ii}(t,\phi_o) = \bar{\epsilon}_{ii}(t,\phi_o) - \alpha_i^*(t,\phi_o)\cdot\phi_o \qquad (i=1,2) \tag{2.1.20}$$

where $\alpha_1^* = \alpha_L^*$ and $\alpha_2^* = \alpha_T^*$, and the subscript i is not summed. Then from (2.1.18), at $\phi = \phi_R$ we get

$$S_{11}^*(0) = \frac{\hat{\epsilon}_{11}(0,\phi_R)}{\sigma_L} \tag{2.1.21}$$

and

$$\Delta S_{11}^{*}(t) = \frac{\hat{\epsilon}_{11}(t,\phi_R) - \hat{\epsilon}_{11}(0,\phi_R)}{\sigma_L} \qquad (2.1.22)$$

Then at $\phi = \phi_o$,

$$V_{11}^{*}(\phi_o) = \frac{\hat{\epsilon}_{11}(0,\phi_o)}{S_{11}^{*}(0)\sigma_L} \qquad (2.1.23)$$

and at some other time $t = \hat{t}$,

$$\Delta S_{11}^{*}(h_{11}^{*}(\phi_o)\cdot\hat{t}) = \frac{\hat{\epsilon}_{11}(\hat{t},\phi_o) - \hat{\epsilon}_{11}(0,\phi_o)}{\sigma_L} - \Delta S_{11}^{*}(\xi_{11}) \qquad (2.1.24)$$

from which

$$h_{11}^{*}(\phi_o) = \xi_{11}/\hat{t} \qquad (2.1.25)$$

From (2.1.19)

$$S_{12}^{*}(0) = \frac{\hat{\epsilon}_{22}(0,\phi_R)}{\sigma_L} \qquad (2.1.26)$$

and

$$\Delta S_{12}^{*}(t) = \frac{\hat{\epsilon}_{22}(t,\phi_R) - \hat{\epsilon}_{22}(0,\phi_R)}{\sigma_L} \qquad (2.1.27)$$

At $\phi = \phi_o$,

$$V_{12}^{*}(\phi_o) = \frac{\hat{\epsilon}_{22}(0,\phi_o)}{S_{12}^{*}(0)\sigma_L} \tag{2.1.28}$$

and at some other time $t = \hat{t}$,

$$\Delta S_{12}^{*}(h_{12}^{*}(\phi_o)\cdot\hat{t}) = \frac{\hat{\epsilon}_{22}(\hat{t},\phi_o)-\hat{\epsilon}_{22}(0,\phi_o)}{\sigma_L} - \Delta S_{12}^{*}(\xi_{12}) \tag{2.1.29}$$

from which

$$h_{12}^{*}(\phi_o) = \xi_{12}/\hat{t} \tag{2.1.30}$$

Now consider the case of an applied transverse isotropic stress

$$\bar{\sigma}_T = \bar{\sigma}_{22} = \bar{\sigma}_{33} \tag{2.1.31}$$

coupled with a uniform temperature distribution, with all other stresses zero. Again simulating an isothermal creep test, we apply the loads

$$\bar{\sigma}_{22}(t) = \bar{\sigma}_{33}(t) = H(t)\sigma_T$$

$$\phi(t) = H(t)\phi_o \tag{2.1.32}$$

Using the first of the stress-strain relations (2.1.4), the S_{12}^{*} creep compliance parameters could again be generated, but this will not be repeated here. From either the second or the third of equations (2.1.4), we get

$$\hat{\epsilon}_T(t,\phi_o) = S_{22}^*(0)V_{22}^*(\phi_o)\sigma_T + S_{23}^*(0)V_{23}^*(\phi_o)\sigma_T$$

$$+\Delta S_{22}^*(\xi_{22})\sigma_T + \Delta S_{23}^*(\xi_{23})\sigma_T \tag{2.1.33}$$

At $\phi = \phi_R$ we have

$$S_{22}^*(0)+S_{23}^*(0)+\Delta S_{22}^*(t)+\Delta S_{23}^*(t) = \bar{\epsilon}_T(t,\phi_R)/\sigma_T \tag{2.1.34}$$

At $t = 0$, $\Delta S_{22}^*(0) = \Delta S_{23}^*(0) = 0$ so that

$$S_{22}^*(0)+S_{23}^*(0) = \bar{\epsilon}_T(0,\phi_R)/\sigma_T \tag{2.1.35}$$

and for $t \neq 0$,

$$\Delta S_{22}^*(t)+\Delta S_{23}^*(t) = \frac{\bar{\epsilon}_T(t,\phi_R)-\bar{\epsilon}_T(0,\phi_R)}{\sigma_T} \tag{2.1.36}$$

For $\phi = \phi_o$ and $t = 0$,

$$S_{22}^*(0)V_{22}^*(\phi_o)+S_{23}^*(0)V_{23}^*(\phi_o)=\hat{\epsilon}_T(0,\phi_o)/\sigma_T \tag{2.1.37}$$

and at $\phi = \phi_o$, $t = \hat{t}$ we get

$$\Delta S_{22}^*(h_{22}^*(\phi_o)\cdot\hat{t})+\Delta S_{23}^*(h_{23}(\phi_o)\cdot\hat{t}) = \frac{\hat{\epsilon}_T(t,\phi_o)-\hat{\epsilon}_T(0,\phi_o)}{\sigma_T} \tag{2.1.38}$$

Now, from transverse shear isothermal creep tests we get the equations

$$S_{55}^{*}(0) - S_{22}^{*}(0) - S_{23}^{*}(0) = 2\bar{\epsilon}_{23}(0,\phi_R)/\sigma_{23} \qquad (2.1.39)$$

$$\Delta S_{55}^{*}(t) - \Delta S_{22}^{*}(t) - \Delta S_{23}^{*}(t) = \frac{2\bar{\epsilon}_{23}(t,\phi_R) - 2\bar{\epsilon}_{23}(0,\phi_R)}{\sigma_{23}} \qquad (2.1.40)$$

For $\phi = \phi_o$ and $t = 0$,

$$S_{22}^{*}(0)V_{22}^{*}(\phi_o) - S_{23}^{*}(0)V_{23}^{*}(\phi_o) = 2\bar{\epsilon}_{23}(0,\phi_o)\sigma_{23} \qquad (2.1.41)$$

and for $t = \hat{t}$,

$$\Delta S_{22}^{*}(h_{22}^{*}(\phi_o)\cdot\hat{t}) - \Delta S_{23}^{*}(h_{23}^{*}(\phi_o)\cdot\hat{t}) = \frac{2\hat{\epsilon}_{23}(t,\phi_o) - 2\hat{\epsilon}_{23}(0,\phi_R)}{\sigma_{23}} \qquad (2.1.42)$$

From (2.1.35) + (2.1.39),

$$S_{22}^{*}(0) = 1/2\left\{\frac{\bar{\epsilon}_T(0,\phi_R)}{\sigma_T} + \frac{2\bar{\epsilon}_{23}(0,\phi_R)}{\sigma_{23}}\right\} \qquad (2.1.43)$$

From (2.1.35) - (2.1.39),

$$S_{23}^{*}(0) = 1/2\left\{\frac{\bar{\epsilon}_T(0,\phi_R)}{\sigma_T} - \frac{2\bar{\epsilon}_{23}(0,\phi_R)}{\sigma_{23}}\right\} \qquad (2.1.44)$$

From (2.1.36) + (2.1.40),

$$\Delta S_{22}^{*}(t) = 1/2\left\{\frac{\bar{\epsilon}_T(t,\phi_R) - \bar{\epsilon}_T(0,\phi_R)}{\sigma_T} + \frac{2\bar{\epsilon}_{23}(t,\phi_R) - 2\bar{\epsilon}_{23}(0,\phi_R)}{\sigma_{23}}\right\} \qquad (2.1.45)$$

From (2.1.36) - (2.1.40),

$$\Delta S_{23}^{*}(t)=1/2\left\{\frac{\bar{\epsilon}_T(t,\phi_R)-\bar{\epsilon}_T(0,\phi_R)}{\sigma_T}-\frac{2\bar{\epsilon}_{23}(t,\phi_R)-2\bar{\epsilon}_{23}(0,\phi_R)}{\sigma_{23}}\right\} \quad (2.1.46)$$

From (2.1.37) + (2.1.41),

$$V_{22}^{*}(\phi_o)=-\frac{1}{2S_{22}^{*}(\phi_o)}\left\{\frac{\hat{\epsilon}_T(0,\phi_o)}{\sigma_T}+\frac{2\bar{\epsilon}_{23}(0,\phi_R)}{\sigma_{23}}\right\} \quad (2.1.47)$$

and (2.1.37) - (2.1.41) gives,

$$V_{23}^{*}(\phi_o)=-\frac{1}{2S_{23}^{*}(\phi_o)}\left\{\frac{\hat{\epsilon}_T(0,\sigma_o)}{\sigma_T}-\frac{2\bar{\epsilon}_{23}(0,\phi_o)}{\sigma_{23}}\right\} \quad (2.1.48)$$

Then (2.1.38) + (2.1.42) results in

$$S_{22}^{*}(h_{22}^{*}(\phi_o)\cdot\hat{t})=1/2\left\{\frac{\hat{\epsilon}_T(t,\phi_o)-\hat{\epsilon}_T(0,\phi_o)}{\sigma_T}+\frac{2\bar{\epsilon}_{23}(t.\phi_o)-2\bar{\epsilon}_{23}(0,\phi_o)}{\sigma_{23}}\right\} \quad (2.1.49)$$

$$=\Delta S_{22}^{*}(\xi_{22})$$

giving

$$h_{22}^{*}(\phi_o)=\xi_{22}/\hat{t} \quad (2.1.50)$$

From (2.1.38) - (2.1.42) we get

$$\Delta S_{23}^{*}(h_{23}^{*}(\phi_o)\cdot\hat{t}) = 1/2\left\{\frac{\hat{\epsilon}_T(t,\phi_o)-\hat{\epsilon}_T(0,\phi_o)}{\sigma_T} - \frac{2\bar{\epsilon}_{23}(t,\phi_o)-2\bar{\epsilon}_{23}(0,\phi_o)}{\sigma_{23}}\right\} \tag{2.1.51}$$

$$= \Delta S_{23}^{*}(\xi_{23})$$

from which

$$h_{23}^{*}(\phi_o) = \xi_{23}/\hat{t} \tag{2.1.52}$$

Now consider the case where thermal loads alone act on the composite cylinder. In the case of a temperature step function rise $\Delta\phi$ relative to the reference temperature ϕ_R, the effective longitudinal secant expansion coefficient α_T^* is defined by ϵ_L while the transverse expansion coefficient α_T^* is defined by the radial surface displacement per unit radius. Thus

$$\alpha_L^*(t,\phi_R,\Delta\phi) = \bar{\epsilon}_L(t)/\Delta\phi$$

(2.1.53)

$$\alpha_T^*(t,\phi_R,\Delta\phi) = \bar{\epsilon}_T(t)/\Delta\phi$$

Schapery [2] proposes that for the thermorheologically simple material (TSM), in the absence of mechanical loads,

$$\bar{\epsilon}_{11} = \int_{-\infty}^{t} \alpha_L^*(\xi_L - \xi_L')\,\frac{d\Delta\phi(\tau)}{d\tau}\,d\tau \tag{2.1.54}$$

$$\bar{\epsilon}_{22}-\bar{\epsilon}_{33}=\int_{-\infty}^{t} \alpha_T^*(\xi_T-\xi_T')\frac{d\Delta\phi(\tau)}{d\tau}d\tau \qquad (2.1.55)$$

where

$$\xi_L=\int_o^t h_L[\phi(\tau)]d\tau \qquad (2.1.56)$$

and

$$\xi_T=\int_o^t h_T[\phi(\tau)]d\tau \qquad (2.1.57)$$

For the most simple of the TCM forms, it is proposed that for a general temperature history, again in the absence of applied stress for convenience,

$$\bar{\epsilon}_{11}(t) = \alpha_L^*(0)V_L^*(\phi)\Delta\phi(t) + \Delta\alpha_L^*(\xi_L)\Delta\phi(0)$$

$$+ \int_{o+}^{t}\Delta\alpha_L^*(\xi_L-\xi_L')\frac{d\Delta\phi}{d\tau}d\tau \qquad (2.1.58)$$

$$\bar{\epsilon}_{22}(t) = \bar{\epsilon}_{33}(t) = \alpha_T^*(0)V_T^*(\phi)\Delta\phi(t) + \Delta\alpha_T^*(\xi_T)\Delta\phi(0)$$

$$+ \int_{o+}^{t} \Delta\alpha_T^*(\xi_T-\xi_T')\frac{d\Delta\phi}{d\tau}d\tau \qquad (2.1.59)$$

For a temperature step function rise

$$\Delta\phi(t) = H(t)\ \Delta\phi \qquad (2.1.60)$$

we obtain the strains

$$\bar{\epsilon}_{11}(t) = \left\{\alpha_L^*(0)V_L^*(\phi)+\Delta\alpha_L^*(\xi_L)\right\}\Delta\phi \qquad (2.1.61)$$

$$\bar{\epsilon}_T(t) = \bar{\epsilon}_{22}(t) = \bar{\epsilon}_{33}(t) = \left\{\alpha_T^*(0)V_T^*(\phi)+\Delta\alpha_T^*(\xi_T)\right\}\Delta\phi \qquad (2.1.62)$$

At $t = 0$, $\Delta\alpha_L^*(0) = \Delta\alpha_T^*(0) = 0$ by definition, so

$$\alpha_L^*(0)V_L^*(\phi) = \frac{\epsilon_{11}(0)}{\Delta\phi} \qquad \alpha_T^*(0)V_T^*(\phi) = \frac{\epsilon_T(0)}{\Delta\phi} \qquad (2.1.63)$$

We now define an arbitrary temperature $\phi = \phi_{R\alpha}$ as the effective thermal expansion coefficients' reference temperature. Since $\Delta\phi = 0$ at the reference temperature defined for the composite effective mechanical creep compliances, some other temperature would be more convenient to use for the composite effective thermal expansion coefficients. Since

$$V_L^*(\phi_{R\alpha}) = V_T^*(\phi_{R\alpha}) = h_L^*(\sigma_{R\alpha}) = h_T^*(\phi_{R\alpha}) = 1 \qquad (2.1.64)$$

there results

$$\alpha_L^*(0) = \frac{\bar{\epsilon}_{11}(0,\phi_{R\alpha})}{\Delta\phi} = \frac{\bar{\epsilon}_{11}(0,\phi_{R\alpha})}{\phi_{R\alpha}-\phi_R} \qquad (2.1.65)$$

and similarly

$$\alpha_T^*(0) = \frac{\bar{\epsilon}_T(0,\phi_{R\alpha})}{\phi_{R\alpha}-\phi_R} \qquad (2.1.66)$$

Then at temperature $\phi_o \neq \phi_{R\alpha}$, the vertical shifts are computed:

$$V_L^*(\phi_o) = \frac{\bar{\epsilon}_{11}(0,\phi_o)}{\alpha_L^*(0)\Delta\phi} \qquad V_T^*(\phi_o) = \frac{\bar{\epsilon}_T(0,\phi_o)}{\alpha_T^*(0)\Delta\phi} \tag{2.1.67}$$

where $\Delta\phi = \phi_o - \phi_R$.

Again considering $\phi_{R\alpha}$,

$$\bar{\epsilon}_{11}(t) = \left\{\alpha_L^*(0) + \Delta\alpha_L^*(t)\right\}\Delta\phi$$

$$\bar{\epsilon}_T(t) = \left\{\alpha_T^*(0) + \Delta\alpha_T^*(t)\right\}\Delta\phi \tag{2.1.68}$$

from which the effective delta compliances are defined:

$$\Delta\alpha_L^*(t) = \frac{\bar{\epsilon}_{11}(t,\phi_{R\alpha})}{\Delta\phi} - \alpha_L^*(0) \tag{2.1.69}$$

$$\Delta\alpha_T^*(t) = \frac{\bar{\epsilon}_T(t,\phi_{R\alpha})}{\Delta\phi} - \alpha_T^*(0)$$

Then, at $\phi = \phi_o$ and $t = \hat{t} \neq 0$,

$$\Delta\alpha_L^*(h_L^*(\phi_o)\cdot\hat{t}) = \frac{\bar{\epsilon}_{11}(\hat{t},\phi_o) - \alpha_L^*(0)V_L^*(\phi_o)}{\Delta\phi} - \Delta\alpha_L^*(\xi_L) \tag{2.1.70}$$

$$\Delta\alpha_T^*(h_T^*(\phi_o)\cdot\hat{t}) = \frac{\bar{\epsilon}_T(\hat{t},\phi_o) - \alpha_T^*(0)V_T^*(\phi_o)}{\Delta\phi} - \Delta\alpha_T^*(\xi_T)$$

from which

$$h_L^*(\phi_o) = \xi_L/\hat{t} \tag{2.1.71}$$

and

$$h_T^*(\phi_o) = \xi_T/\hat{t} \tag{2.1.72}$$

2.2. LITERATURE SURVEY OF THERMOVISCOELASTIC MATERIAL PROPERTIES

As part of this work, an extensive literature search was conducted in an effort to determine realistic material properties of thermoviscoelastic solids, in particular those typically employed as epoxy matrices in composites. Several papers, e.g. [3-8], were found which provided some or all of the material parameters for a thermorheologically simple characterization of typical matrix material. However, very little data exists for thermorheologically complex viscoelastic epoxies.

A number of papers [9-13] and a private communication [14] were obtained which provided useful data on thermorheologically complex epoxy matrices. All of the papers [9-13] used a characterization scheme which fitted the data to a semi-empirical model first developed by Schapery [15] for nonlinear isothermal viscoelasticity. The data in all of these papers, first reported in [9] and [10], was modified for use in the work reported here, as described in a previous report [16].

The matrix thermoviscoelastic data used in this study, including the time-dependent matrix shear creep compliance, the matrix shear horizontal shift and vertical shift, are included in Figures 2.1, 2.2 and 2.3, respectively. The fiber elastic properties and the matrix properties at reference temperature are listed in Table 1.

2.3. EVALUATION OF EFFECTIVE THERMOVISCOELASTIC PARAMETERS

Note that in the equations of Section 2.1, the stresses and temperatures are applied, and the composite or average strains are assumed

to be known so that the effective compliance parameters may be calculated. The analytical tools available for generating average strains in composite cylinders involving transversely isotropic fibers and an isotropic matrix include the composite cylinder assemblage (CCA) model and the analysis of a periodic hexagonal array [17]. The details regarding the analysis for average strains in a composite cylinder composed of transversely isotropic temperature-dependent elastic fibers and a thermorheologically complex viscoelastic matrix were developed in the Phase I portion of this effort [16]. Average strains due to thermal expansion and axisymmetric mechanical loadings were examined with the composite cylinder assemblage model, while transverse loading effects were analyzed using a finite element model of a periodic hexagonal array.

Numerical simulations of the series of isothermal creep tests described in Section 2.1 were performed in each mode of deformation, to determine the complete set of effective creep compliance parameters of the composite constitutive equations. Figures 2.1 through 2.3 show the time dependent creep compliance, horizontal shift and vertical shift, respectively, for the composite axial deformation compliance. Since this deformation mode is largely dominated by the elastic fibers, the creep compliance (Figure 2.1) is several orders of magnitude less than that of the matrix shear creep compliance. This fiber dominance also manifests itself in the shifts (Figures 2.2 and 2.3) through a much more shallow slope in the composite shift curves than in the matrix shift curves. Figures 2.4 through 2.6 show the time dependent creep compliance, horizontal shift and vertical shift, respectively, for the composite axial shear compliance. Since in this mode, the matrix participation is dominant, the composite parameters are much closer to the matrix values.

2.4. VERIFICATION OF EFFECTIVE COMPOSITE CONSTITUTIVE EQUATIONS

The macromechanical response of a composite structural element, as predicted by the effective constitutive equations and their derived parameters, was checked against results computed using a micromechanical model (composite cylinder assemblage) which explicitly included the fiber and matrix as discrete phases. A slowly varying periodic shear stress was applied to the composite in the presence of an oscillating temperature. It

should be noted that even though the composite cylinder assemblage model was used to generate the parameters of the effective thermoviscoelastic equations, this model can still be used to verify the equations and their parameters for arbitrary time varying mechanical and temperature loadings, since the parameters were generated using a series of isothermal creep tests.

The simultaneously applied axial stress history and temperature load are shown in Figures 2.7 and 2.8, respectively. Comparisons of the axial shear strains and the thermally induced longitudinal and transverse strains for this loading are shown in Figures 2.9, 2.10 and 2.11 respectively. Note that essentially identical results for all of the strains were obtained from the macro- and micromechanical models, thereby verifying both the assumed form and the individual parameters of the composite constitutive equations.

The significance of the verification, illustrated in Figures 2.9 through 2.11, is that it allows structural analyses involving TCM composites to be performed in an efficient manner, namely by simply using the effective constitutive equations. If these equations could not be verified, the response of the composite element would have to be computed at each time step by using both the CCA model and the finite element model of the hexagonal array, both of which require the solution of simultaneous algebraic equations, just to evaluate the average strain field in the composite due to the applied mechanical and thermal loads. This would be an extremely tedious and computationally excessive process for any practical structural analysis involving TCM composites.

3. RESPONSE TO SINUSOIDAL TEMPERATURE AND LOAD

In isothermal viscoelasticity, the application of a sinusoidal stress results in a sinusoidal strain at the same frequency. The oscillating stress and strain reach their peak values at different times, i.e. there is a phase shift between stress and strain. This can be seen in Figures 3.1 and 3.2 which show respectively a sinusoidal axial shear stress history applied isothermally and the resulting axial shear strain. The strain response is most conveniently characterized using a complex compliance, where the real part is the ratio of the strain amplitude to stress amplitude, and the imaginary part represents the phase shift. At the frequency of the applied stress shown in Figure 3.1, both the real and imaginary parts of the complex compliance can be computed using the information on the peak magnitudes and the time difference between the peaks shown in Figures 3.1 and 3.2. In the general case, both the real and imaginary parts are functions of the frequency of the applied stress.

The purpose of analyzing the effects of simultaneous sinusoidal temperature and load was to determine if a periodic response was obtained for the composite, and if so, to examine the form of the periodic response. In particular it was of interest to determine if a complex compliance existed in this situation.

Several cases were run involving the application of a sinusoidal shear stress and a sinusoidal temperature at different frequencies. Figure 3.3 shows the resulting axial shear strain for the case where the shear stress frequency was twice the frequency of the temperature cycle. Figure 3.4 gives the shear strain for the case where the shear stress frequency was two-thirds the applied temperature frequency, and Figure 3.5 gives the shear strain when the shear stress frequency is two-fifths the applied temperature frequency. It is apparent from all of these curves that the steady state portion of the strain can be decomposed into two sinusoidal components, whose frequencies are equal to the applied stress frequency and the temperature frequency. This implies the existence of a two frequency complex compliance which, from a computational point of view, could be developed into a powerful tool for performing structural dynamic analysis of TSM and TCM structures under arbitrary mechanical and thermal loading conditions.

4. DYNAMIC ANALYSES OF THERMOVISCOELASTIC COMPOSITE STRUCTURES

4.1. INTRODUCTION

The purpose of this section is to present the results of the effects of thermoviscoelastic behavior on the damped response of some simple composite structures. Two separate problems were considered: the free vibration of a cantilevered unidirectional beam of cylindrical cross-section, and the response of a simple truss to impulsive mechanical loading in the presence of isothermal and transient temperature conditions. The role of shear deformation is demonstrated in the free vibration study, and the influence of matrix deformation on damped response is shown in the truss problems.

4.2. FREE FLEXURAL VIBRATIONS OF CANTILEVERED UNIDIRECTIONAL BEAM

As an initial illustration of dynamic analysis of a TCM composite structure, we consider the case of free flexural vibrations of a cantilevered beam which is uniaxially reinforced in the beam axis direction. As mentioned above, the purpose of the investigation is to compare vibration damping due to matrix thermoviscoelasticity on the basis of the usual theory which neglects the effect of shear, and on the basis of the more refined Timoshenko theory which takes into account shear as well as rotatory inertia. Recall that the loss tangent is defined as the ratio of the imaginary part of the complex modulus to its real part. For isotropic materials, in which the complex Young's modulus loss tangent and the complex shear modulus loss tangent are of the same order, the added effect of shear and rotatory inertia is small for vibration modes of low order and for long beams. In the present case, however, where the axial Young's modulus loss tangent is by an order of magnitude smaller than that of the axial shear modulus, the situation is quite different as will be shown.

Considering only the effect of flexure, by the correspondence principle for viscoelastic vibrations [18], the differential equation for the transverse deflection y of a freely vibrating beam is

$$\tilde{E}_A(\omega) I \frac{\partial^4 y}{\partial x^4} + \rho A \frac{\partial^2 y}{\partial t^2} = 0 \qquad (4.2.1)$$

where

$\tilde{E}_A(\omega) = E_A^R(\omega) + iE_A^I(\omega)$ = complex axial Young's modulus,

I = moment of inertia

A = area of the cross section

ρ = density.

By the conventional separation of variables method, the solution to the governing partial differential equation (4.2.1) is given by

$$y(x,t) = (A_1 \sin ax + A_2 \cos ax + A_3 \sinh ax + A_4 \cosh ax) e^{i\tilde{\omega}t} \qquad (4.2.2)$$

with

$$a^4 = \rho A \tilde{\omega}^2 / \tilde{E}_A I \qquad (4.2.3)$$

where the constants A_i are evaluated from boundary conditions on a cantilevered beam

$$y(0,t) = 0$$

$$y'(0,t) = 0 \qquad (4.2.4)$$

$$M(L,t) = \tilde{E}_A I y''(L,t) = 0$$

$$V(L,t) = \tilde{E}_A I y'''(L,t) = 0$$

Substituting the solution given by (4.2.2) into the homogeneous boundary conditions, by requiring a non-trivial solution for at least one of the constants, leads to the frequency equation

$$1 + \cos aL \cosh aL = 0 \tag{4.2.5}$$

The solution to this transcendental equation will be represented as $a_n L$ so that the beam natural frequencies may be obtained from the solution of

$$\tilde{\omega}_n = a_n^2 \cdot (\tilde{E}_A(\omega) I/\rho A)^{1/2} \tag{4.2.6}$$

Note that in the elastic case, the natural frequencies are obtained by simply evaluating the right hand side of (4.2.6). However in the viscoelastic case, since $\tilde{E}_A$ is a function of frequency, equation (4.2.6) is nonlinear in frequency and thus the real and imaginary parts must be obtained in an iterative fashion.

The time varying portion of the solution takes the form

$$e^{i\tilde{\omega}_n t} = e^{i\omega_n^R t} \; e^{-\omega_n^I t} \tag{4.2.7}$$

Thus the real part of each natural frequency represents the oscillatory component and the imaginary part is the attenuation, a measure of the damping introduced by the viscoelastic matrix material.

Next the same beam is considered in Timoshenko fashion, with shear and rotatory inertia. Again using the correspondence principle, the coupled equations for the total deflection y and bending slope ψ are given by Timoshenko [19] as

$$\tilde{E}_A I \frac{\partial^2 \psi}{\partial x^2} + k\left(\frac{\partial y}{\partial x} - \psi\right) A\tilde{G}_A - \rho I \frac{\partial^2 \psi}{\partial t^2} = 0 \tag{4.2.8}$$

$$\rho A\frac{\partial^2 y}{\partial t^2} - k\left[\frac{\partial^2 y}{\partial x^2} - \frac{\partial \psi}{\partial x}\right]A\tilde{G}_A = 0 \qquad (4.2.9)$$

where the new constants are

$\tilde{G}_A(\omega) = G_A^R(\omega) + iG_A^I(\omega)$ = the axial complex shear modulus, and

k = a numerical shape factor for the cross section.

Following the development first shown in Huang [20], we eliminate ψ or y from equations (4.2.8) and (4.2.9) and obtain the two uncoupled differential equations in y and ψ

$$\tilde{E}_A I\frac{\partial^4 y}{\partial x^4} + \rho A\frac{\partial^2 y}{\partial t^2} - \rho I\left[1 + \frac{\tilde{E}_A}{k\tilde{G}_A}\right]\frac{\partial^4 y}{\partial x^2 \partial t^2} + \frac{\rho^2 I}{k\tilde{G}_A}\frac{\partial^4 y}{\partial t^4} = 0 \qquad (4.2.10)$$

$$\tilde{E}_A I\frac{\partial^4 \psi}{\partial x^4} + \rho A\frac{\partial^2 \psi}{\partial t^2} - \rho I\left[1 + \frac{\tilde{E}_A}{k\tilde{G}_A}\right]\frac{\partial^4 \psi}{\partial x^2 \partial t^2} + \frac{\rho^2 I}{k\tilde{G}_A}\frac{\partial^4 \psi}{\partial t^4} = 0 \qquad (4.2.11)$$

Introducing the nondimensional parameter $\theta = x/L$ and assuming solutions to be of the form

$$y = Ye^{i\tilde{\omega}t} \qquad (4.2.12)$$

$$\psi = \Psi e^{i\tilde{\omega}t}$$

equations (4.2.8) to (4.2.11) take the form

$$\tilde{S}^2\Psi'' - (1-\tilde{b}^2 r^2\tilde{S}^2)\Psi + Y'/L = 0 \qquad (4.2.13)$$

$$Y'' + \tilde{b}^2\tilde{S}^2 Y - L\Psi' = 0 \tag{4.2.14}$$

$$Y^{IV} + \tilde{b}^2(r^2+\tilde{S}^2)Y'' - \tilde{b}^2(1-\tilde{b}^2 r^2\tilde{S}^2)Y = 0 \tag{4.2.15}$$

$$\Psi^{IV} + \tilde{b}^2(r^2+\tilde{S}^2)\Psi'' - \tilde{b}^2(1-\tilde{b}^2 r^2\tilde{S}^2)\Psi = 0 \tag{4.2.16}$$

where

$$\tilde{b}^2 = \frac{\rho A}{\tilde{E}_A I} L^4 \tilde{\omega}^2 \tag{4.2.17}$$

$$r^2 = I/AL^2 \tag{4.2.18}$$

$$\tilde{S}^2 = \tilde{E}_A I/kA\tilde{G}_A L^2 \tag{4.2.19}$$

and the primes for Y and Ψ represent differentiation with respect to θ. At the clamped end of the beam we have the boundary conditions

$$\begin{aligned} \Psi &= 0 \\ Y &= 0 \end{aligned} \tag{4.2.20}$$

and at the free end we have

$$\begin{aligned} \Psi' &= 0 \\ \frac{1}{L}Y' - \Psi' &= 0 \end{aligned} \tag{4.2.21}$$

The solutions to (4.2.15) and (4.2.16) can be found as

$$Y = C_1 \cosh \tilde{b}\tilde{\alpha}\theta + C_2 \sinh \tilde{b}\tilde{\alpha}\theta + C_3 \cos \tilde{b}\tilde{\beta}\theta + C_4 \sin \tilde{b}\tilde{\beta}\theta \quad (4.2.22)$$

$$\Psi = C_5 \cosh \tilde{b}\tilde{\alpha}\theta + C_6 \sinh \tilde{b}\tilde{\alpha}\theta + C_7 \cos \tilde{b}\tilde{\beta}\theta + C_8 \sin \tilde{b}\tilde{\beta}\theta \quad (4.2.23)$$

where

$$\tilde{\alpha},\ \tilde{\beta} = \frac{1}{\sqrt{2}} \left\{ -,+(r^2+\tilde{s}^2)+[(r^2-\tilde{s}^2)^2 + 4/\tilde{b}^2]^{1/2} \right\}^{1/2} \quad (4.2.24)$$

Note that only half of the constants in equations (4.2.22) and (4.2.23) are independent. The constants C_5 through C_8 may be related to C_1 through C_4 using equations (4.2.13) or (4.2.14).

From the requirement that a non-trivial solution exist for at least one of the constants, using the appropriate boundary conditions (4.2.20) and (4.2.21) within (4.2.22) and (4.2.23) we get as a frequency equation

$$2+\left[\tilde{b}^2(r^2-\tilde{s}^2)^2+2\right]\cosh \tilde{b}\tilde{\alpha} \cos \tilde{b}\tilde{\beta} - \frac{\tilde{b}(r^2+\tilde{s}^2)}{(1-\tilde{b}^2 r^2 \tilde{s}^2)^{1/2}} \sinh \tilde{b}\tilde{\alpha} \sin \tilde{b}\tilde{\alpha} = 0 \quad (4.2.25)$$

As with (4.2.6) above, a nonlinear solution technique must be used on (4.2.25) to obtain the real and imaginary components of the beam natural frequencies.

To use the natural frequency equations given above, the effective complex Young's modulus and the effective complex axial shear modulus for the unidirectional composite must be known. These were generated in a manner entirely analogous to that used in Section 2 in generating the effective creep compliance parameters of the composite. In this case, however, instead of dealing with "reduced time" as the independent variable of the time dependent creep compliances, we work with "reduced frequency" as the abscissa of the complex moduli. As with the creep compliances, the horizontal shifts are used to compute the reduced frequency for the complex moduli.

As an illustration of the dependence of response on temperature, the natural frequencies of a fixed-free carbon-epoxy unidirectional tube 40 inches long, 0.01 inch in thickness, and 1 inch in diameter were obtained by

solving the frequency equations (4.2.6) and (4.2.25) under isothermal conditions. As with the earlier examples, T300 fibers were embedded with a volume fraction of 0.6 within a Hercules 3502 epoxy resin matrix.

Figure 4.1 shows the first mode natural frequencies for the carbon-epoxy cantilevered beam as a function of temperature. This curve shows that the real part, or resonant frequency, is essentially independent of temperature and, in addition, is practically unchanged by the presence of shear deformation and rotatory inertia. The imaginary or attenuation component varies considerably with temperature, however, and is strongly affected by shear deformation. The effects of shear deformation can be readily seen in Figure 4.2, which shows the envelopes of the first mode response of both beam models at room temperature. Figure 4.3 shows the second mode natural frequencies for the beam as a function of temperature. For the Bernoulli-Euler beam the resonant frequency remains independent of temperature, but both shear deformation and temperature have an effect on the second resonant frequency, as can be seen by the difference occurring in the real components. Shear deformation effects on the imaginary part are even more pronounced than in the first mode, as can be seen by the increased spread between the two imaginary components. The result of shear deformation on the second mode is even more apparent in Figure 4.4, which shows a significantly shorter decay time for the response of the Timoshenko beam than for the Bernoulli-Euler beam.

4.3. EFFECT OF TRANSIENT LOADS AND TEMPERATURES ON A SIMPLE COMPOSITE STRUCTURE

As a second illustration of dynamic analysis of a TCM composite structure, we consider the case of the simple truss shown in Figure 4.5. All three truss members are unidirectional carbon-epoxy composite rods, characterized using TCM behavior. Note from this figure that a zero degree layup is defined as fibers parallel to the axis of the bar and a 90 degree layup is defined as fibers perpendicular to the axis of the bar.

To perform the truss dynamic analyses, rod finite elements were developed using the standard linear displacement field [23] for uniaxial members composed of thermorheologically complex material. The TCM rod elements were then incorporated within a finite element code capable of

performing isothermal natural frequency analysis, as well as static, thermal, and dynamic stress analysis. The dynamic analyses were performed in the time domain using the direct integration procedure of Newmark [24] as outlined by Bathe and Wilson [25].

As a first step towards examining truss response under transient loading conditions, an eigensolution of the two degree-of-freedom truss was performed at a temperature of 117 degrees Kelvin above the reference temperature (303 degrees Kelvin). The mode shapes and natural frequencies resulting from the eigensolution are given in Figure 4.6. The natural frequencies for a truss composed entirely of zero degree layup members and a truss composed entirely of 90 degree layup members are shown in the figure.

The truss was subjected to an impulsive horizontal load 1 kN in magnitude and one second in duration, and the response was examined for isothermal as well as transient temperature conditions applied uniformly over the entire truss. At 117 degrees Kelvin above the reference temperature, Figure 4.7 shows the vertical displacement at the apex (joint 2) of the truss with zero degree layup members. In this truss, most of the load is carried by the fibers, so that there is little matrix deformation occurring during the response. This results in very little damping as shown by the insignificant amount of decay occurring in the one minute of response shown in the figure. For the same loading and at the same temperature, the vertical displacement at joint 2 of the truss with 90 degree layup members is shown in Figure 4.8. In addition to the larger response period, resulting from 90 degree layup members having smaller stiffness than zero degree layup members, a substantial amount of decay in the response is evident from this figure, a direct result of more matrix deformation occurring in this configuration than in the zero degree layup configuration.

For the same impulsive mechanical load, two other thermal load conditions were examined for the truss with 90 degree layup members. The response at the reference temperature as well as the response occurring for the transient temperature condition of $\Delta\phi$ = 117°K x t (min) were both examined. For these two load cases, peak responses were between the limits of the peaks of Figures 4.7 and 4.8. The envelopes of the vertical displacement response histories for all four cases examined are shown in Figure 4.9. Not surprisingly, as in the cantilever free vibration problem,

the amount of damping present in the response is dependent on temperature and the extent of matrix deformation in the composite members.

As a final truss analysis problem, the response of the truss composed entirely of zero degree layup members and with the lumped mass at joint 2 removed, was examined under thermal shock conditions, in the absence of any mechanical loading. A temperature varying linearly from 80°K to 420°K in 0.5 seconds and held constant at 420°K thereafter was used as the thermal load applied uniformly to all members of the truss, as shown in Figure 4.10. The horizontal and vertical displacement histories at joint 2 of the truss are shown in Figures 4.11 and 4.12 respectively. Due to changes in the displacement and velocity occurring rapidly enough for inertia forces to be significant, oscillations occur during the entire response interval examined and, when the temperature becomes constant at 0.5 seconds, the oscillations take place about the displacement reached at that time. The stresses in members 1 and 2 are shown in Figures 4.13 and 4.14 respectively. Since joint 2 is unrestrained, these stresses result only from the oscillations in the displacements occurring at joint 2.

5. DISCUSSION AND RECOMMENDATIONS

The research program detailed in this report has had several significant results, among them the derivation and verification of the composite TCM stress-strain equations, and the demonstration of the significance of temperature and shear deformation on the damped response of TCM composite structures. From the standpoint of performing dynamic analysis on space structures composed of carbon fiber/polymeric matrix composites, the results of applying sinusoidal mechanical and thermal loads on TCM composite structural elements, and observations concerning the computations in the forced vibration analysis of the truss structures were equally important.

As discussed in Section 3, numerical experiments performed indicate the existence of two frequency complex compliances/moduli for thermorheologically complex materials. By analogy to isothermal viscoelastic analysis, this means that for periodic thermal and mechanical loads, the TCM response will be most conveniently obtained by the superposition of the effects due to the applied stress frequency components plus the thermal load frequency components. In other words, for periodic loads, frequency domain response is more efficient.

The dynamic analyses of the truss structure detailed in Section 4 were accomplished by direct time integration of the differential equations of motion. At each time step and for each element, the hereditary integrals must be re-evaluated. In the case of TCM creep compliances represented using power law forms, this is a computationally intensive task which takes more and more effort as the duration of response becomes larger and larger. Consequently for isothermal truss dynamic analyses involving either periodic or non-periodic loads, the complex frequency response method is far more computationally efficient. With the development of the two frequency complex compliances/moduli for TCM members, the complex frequency response method could be extended to allow the solution of periodic and non-periodic thermal and mechanical loads to be performed in the frequency domain. In addition, the versatility gained by using a frequency domain formulation, in particular the ability to perform stochastic analyses, would enhance the attractiveness of this approach.

REFERENCES

1. Flugge, W., Viscoelasticity, Blaisdell Publishing Company, Waltham, Mass., 1967.

2. Shapery, R.A., "Viscoelastic Behavior and Analysis of Composite Materials," in Composite Materials, Vol. 2, Sendeckyj, G.P., ed., Academic Press, pp. 84-168, 1974.

3. Sternstein, S.S. and Yang, P., "Characterization of the Matrix Glass Transition in Carbon-Epoxy Laminates Using the CSD Test Geometry," from The Role of the Polymeric Matrix in the Processing and Structural Properties of Composite Materials, J.C. Seferis and L. Nicolais editors, Plenum Publishing Corp., 1983.

4. Yang, P., Carlsson, L. and Sternstein, S.S., "Dynamic-Mechanical Response of Graphite/Epoxy Composite Laminates and Neat Resin," Polymer Composites, Vol. 4, No. 2, April 1983, pp 104-112.

5. Hurwitz, F.I., "Dynamic Mechanical Characterization of Cure of a Polyimide-Graphite Fiber Composite," Journal of Polymer Composites, Vol. 4, No.2, April 1983, pp 90-97.

6. Moehlenpah, A.E. et al, "The Effect of Time and Temperature on the Mechanical Behavior of Epoxy Composites," Polymer Engineering and Science, Vol. 11, No. 2, March 1971, pp 129-138.

7. Plazek, D.J. "The Temperature Dependence of the Viscoelastic Softening and Terminal Dispersions of Linear Amorphous Polymers," Journal of Polymer Science, Vol. 20, 1982, pp 729-742.

8. Mijovic, J. and Liang, R.C., "The Effect of Pressure and Temperature on Time-Dependent Changes in Graphite/Epoxy Composites Below the Glass Transition," Polymer Engineering and Science, Vol. 24, No. 1, Jan. 1984, pp 57-66.

9. Watkins, L.A., "Creep of an Epoxy Resin Under Transient Temperatures," Masters Thesis in Civil Engineering, Texas A&M University, August 1973.

10. Harper, B.D. and Weitsman, Y., "Characterization of Thermo-Rheologically Complex Materials," J. of Rheology, Vol. 29, No. 1, Feb. 1985, pp 49-68.

11. Weitsman, Y., "Residual Thermal Stresses Due to Cool-Down of Epoxy-Resin Composites," Journal of Applied Mechanics, Vol. 46, Sept. 1979, pp 563-567.

12. Weitsman, Y. and Harper, B.D., "Optimal Cooling of Cross-Ply Composite Laminates and Adhesive Joints," Journal of Applied Mechanics, Vol. 49, Dec. 1982, pp 735-739.

13. Harper, B.D., "Optimal Cooling Paths for a Class of Thermo-Rheologically Complex Materials," Journal of Applied Mechanics, Vol. 52, Sept. 1985, pp 634-638.

14. Private communication from C.J. Aloisio (AT&T Bell Labs) to Z. Hashin, Feb. 18, 1985.

15. Schapery, R.A., Polymer Engineering and Science, Vol. 9, pp 295-310.

16. Hashin, Z., Humphreys, E.A. and Goering, J., "Thermoviscoelastic Analysis of Dimensionally Stable Fiber Composite Space Structures," MSC TFR 1504 to AFOSR, August, 1984.

17. Hashin, Z., "Theory of Fiber Reinforced Materials," NASA CR-1974, March, 1972.

18. Christensen, R.M., Theory of Viscoelasticity: An Introduction, Academic Press, New York, N.Y., 1971.

19. Timoshenko, S., Young, D.H., and Weaver, W., Vibration Problems in Engineering, 4th Edition, John Wiley & Sons, New York, N.Y., 1974.

20. Huang, T.C., "The Effect of Rotatory Inertia and of Shear Deformation on the Frequency and Normal Mode Equations of Uniform Beams with Simple End Conditions," Journal of Applied Mechanics, Trans. ASME, December 1961, pp 579-584.

21. Hashin, Z., "Damping Characteristics of Fiber Composites," Proceedings of the 8th International Congress of the Aeronautical Sciences (ICAS), Amsterdam, 1972.

22. Nakao, T., Okano, T., and Asano, I., "Theoretical and Experimental Analysis of Flexural Vibration of the Viscoelastic Timoshenko Beam," Journal of Applied Mechanics, Vol. 52, September 1985, pp 728-731.

23. Gallagher, R.H., Finite Element Analysis Fundamentals, Prentice-Hall, Englewood Cliffs, N.J., 1975.

24. Newmark, N.M., "A Method of Computation for Structural Dynamics," ASCE Journal of the Engineering Mechanics Division, Vol. 85, 1959, pp 67-94.

25. Bathe, K.-J. and Wilson, E.L., Numerical Methods in Finite Element Analysis, Prentice-Hall, Englewood Cliffs, N.J., 1976.

Table 1. Material Properties

Fiber Properties

E_A = 231 GPA

E_T = 22.4 GPa

G_A = 22.1 GPa

G_T = 8.30 GPa

ν_A = 0.30

α_A = -1.33. μm/m°c

α_T = 7.04 μm/m°c

V_F = 0.60

Matrix properties at reference temperature (303°K)

k = 3.58 GPa

g(o) = 0.606 $(GPa)^{-1}$

ν = 0.30

α = 30.0 μm/m°K

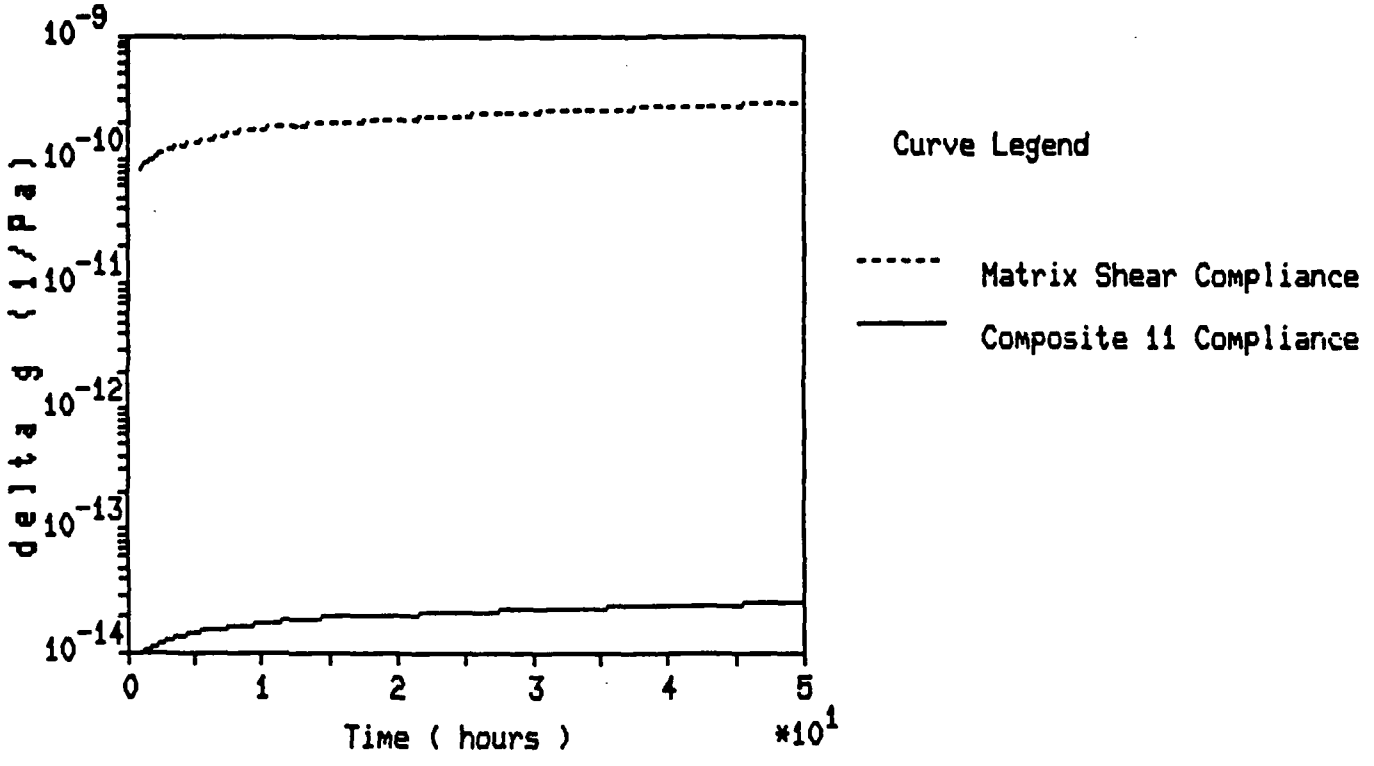

Figure 2.1. Effective Axial Deformation Creep Compliance for Unidirectional Carbon/Epoxy Composite

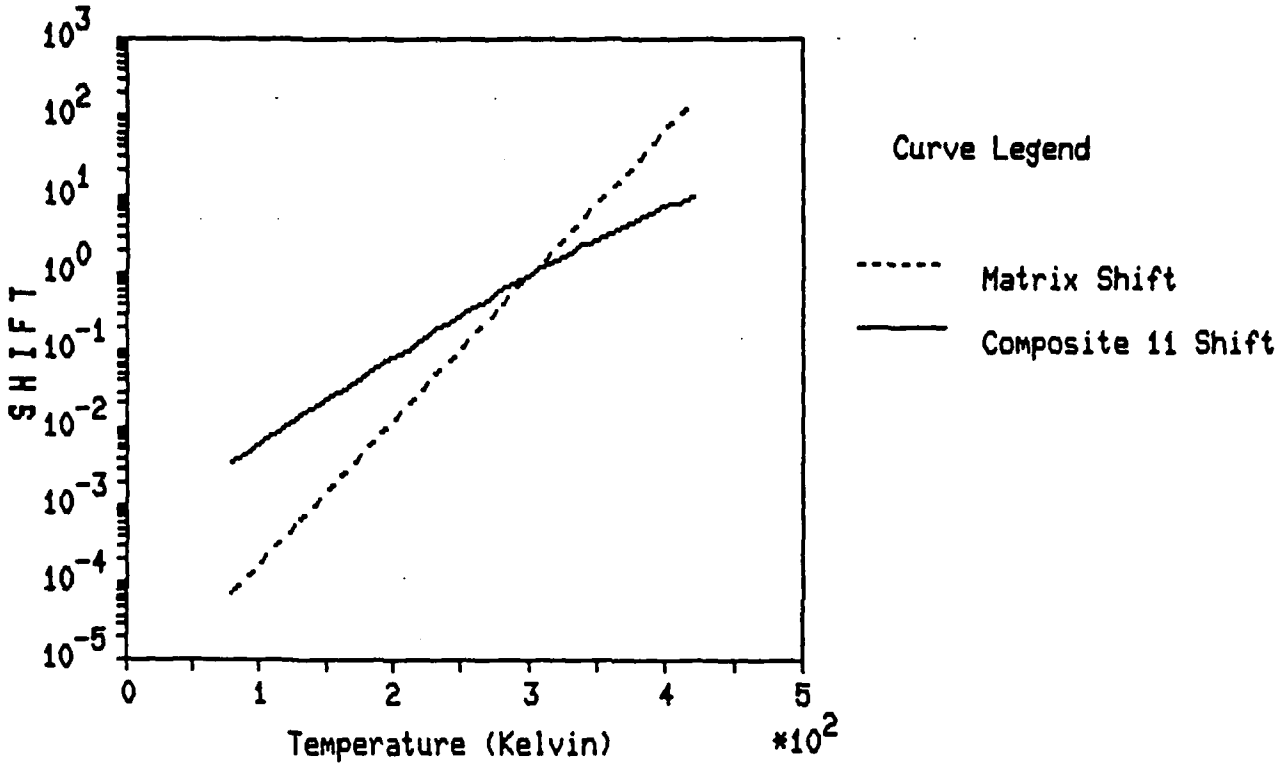

Figure 2.2. Effective Axial Deformation Horizontal Shift for Unidirectional Carbon/Epoxy Composite

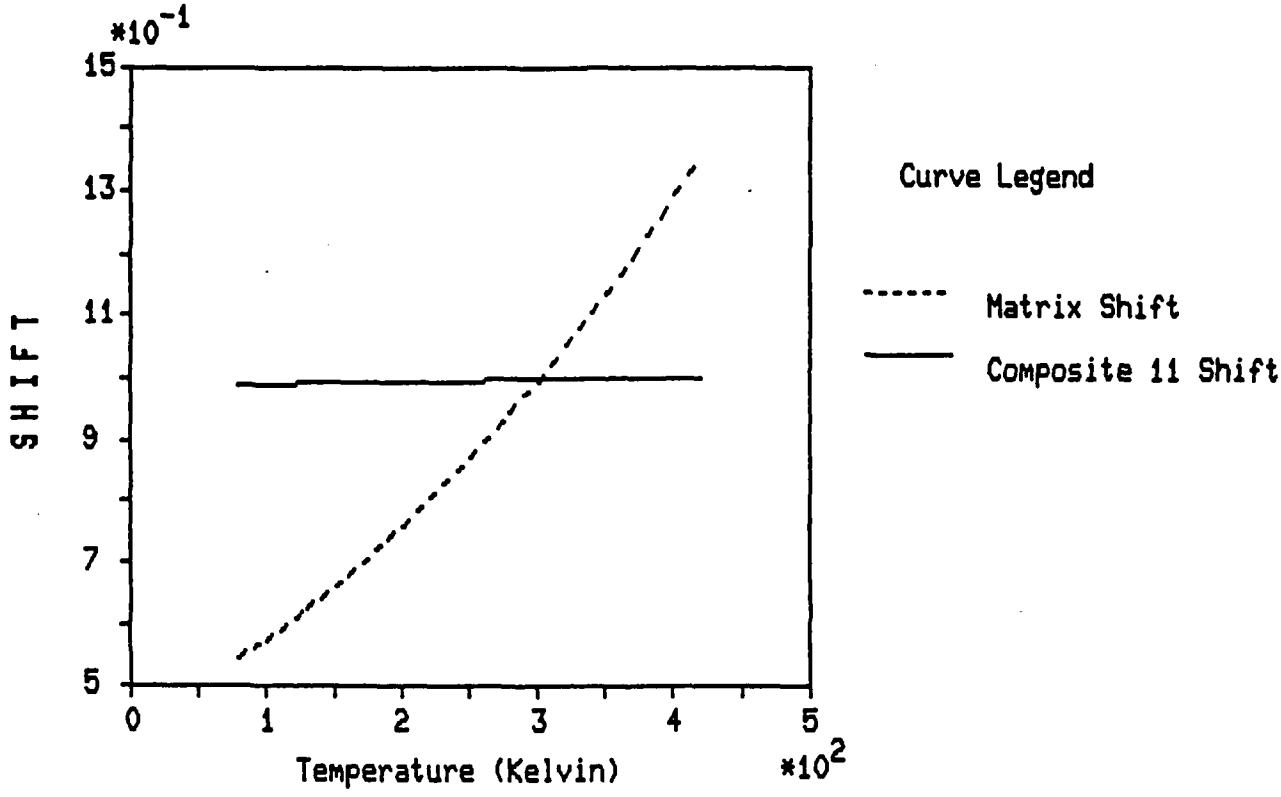

Figure 2.3. Effective Axial Deformation Vertical Shift for Unidirectional Carbon/Epoxy Composite

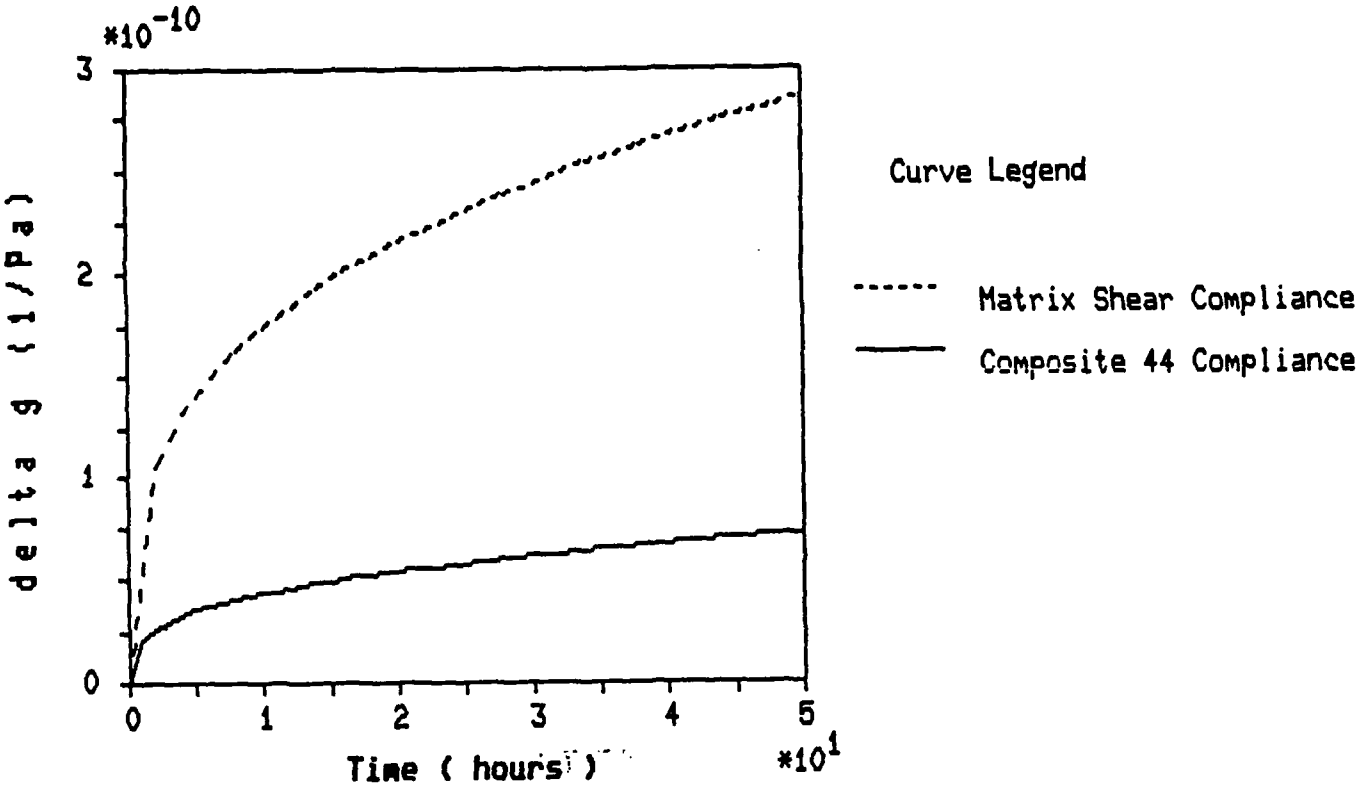

Figure 2.4. Effective Axial Shear Creep Compliance for Unidirectional Carbon/Epoxy Composite

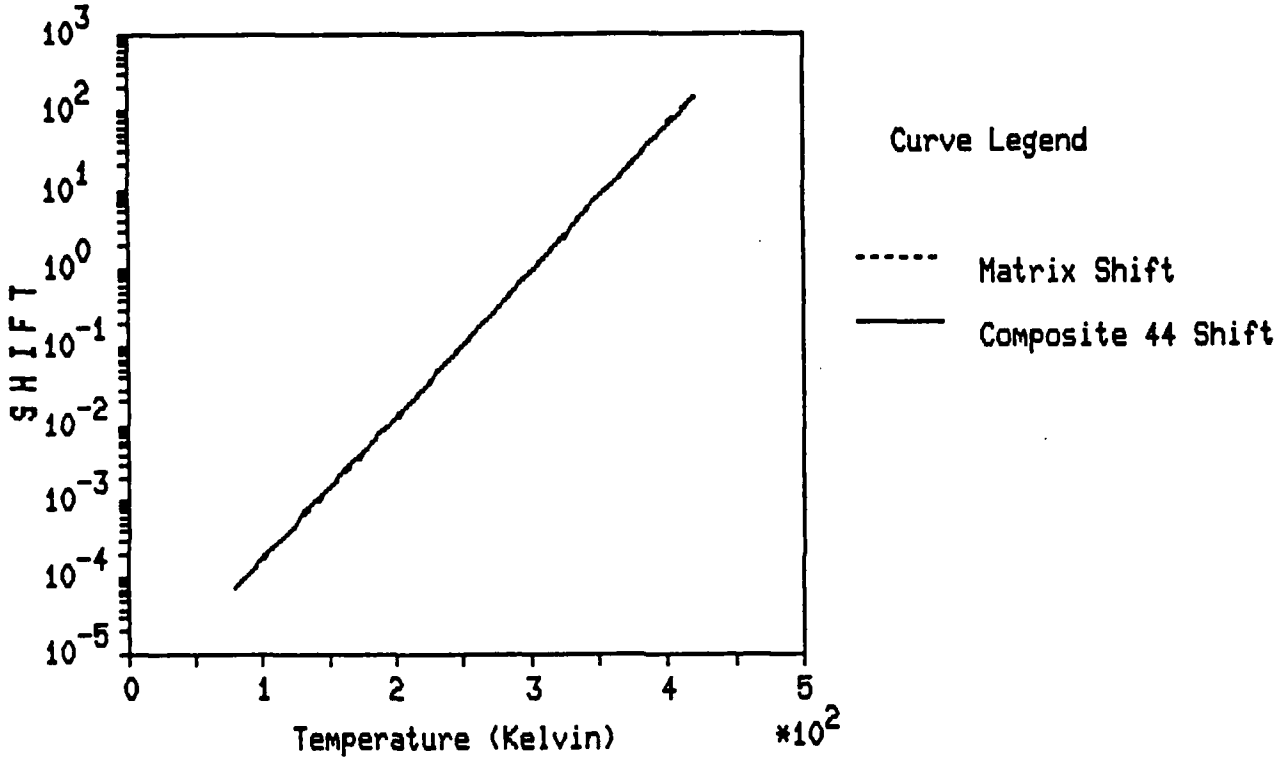

Figure 2.5. Effective Axial Shear Horizontal Shift for Unidirectional Carbon/Epoxy Composite

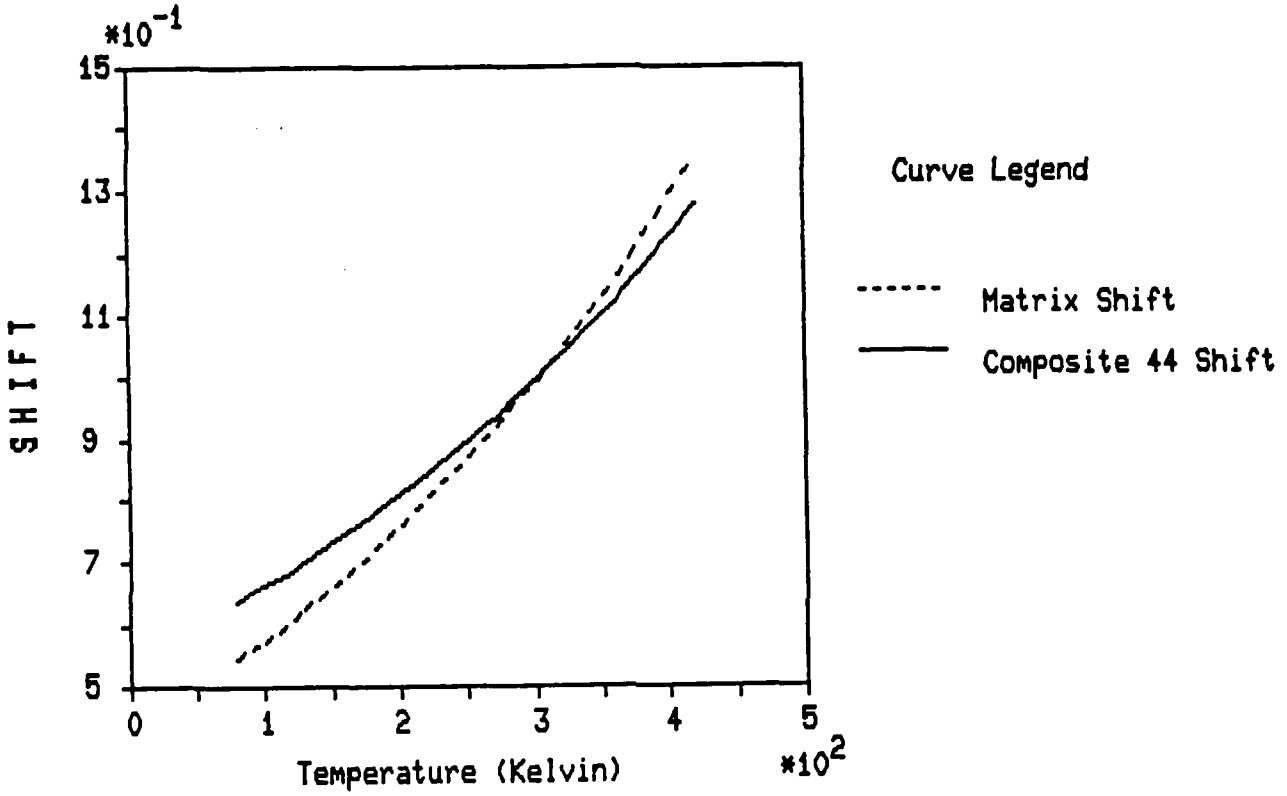

Figure 2.6. Effective Axial Shear Vertical Shift for Unidirectional Carbon/Epoxy Composite

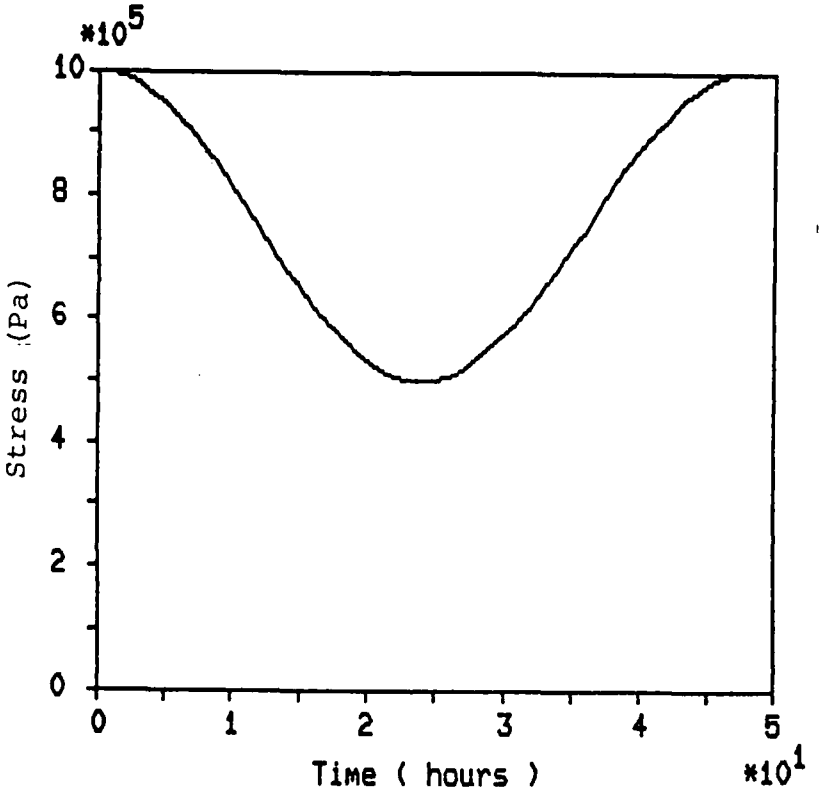

Figure 2.7. Applied Axial Shear Stress History on Unidirectional Carbon/Epoxy Composite Structural Element

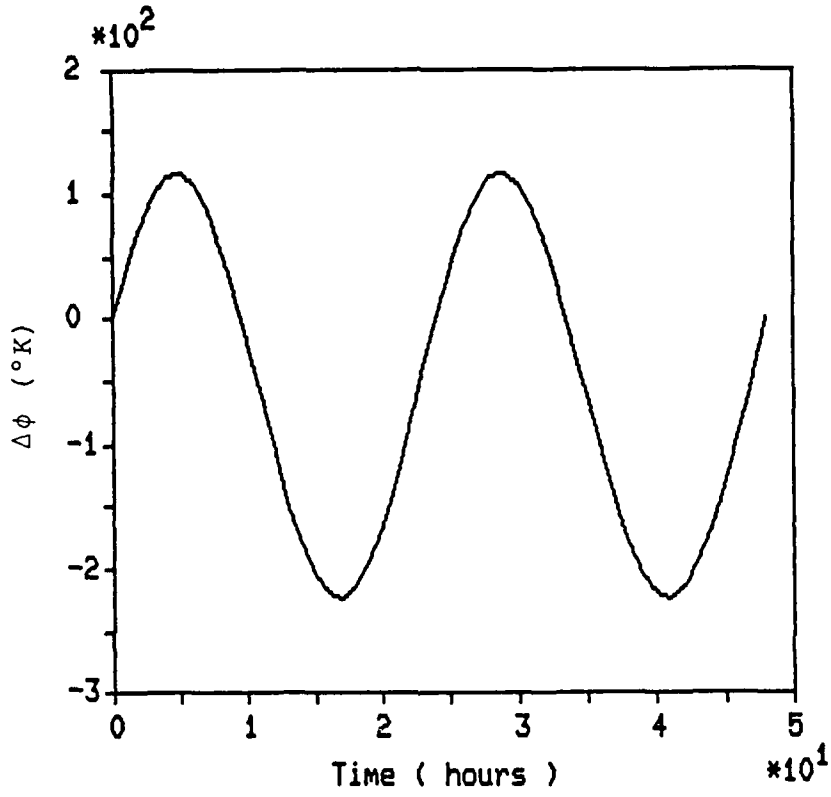

Figure 2.8. Variation in Temperature From 303 Degrees Kelvin Reference

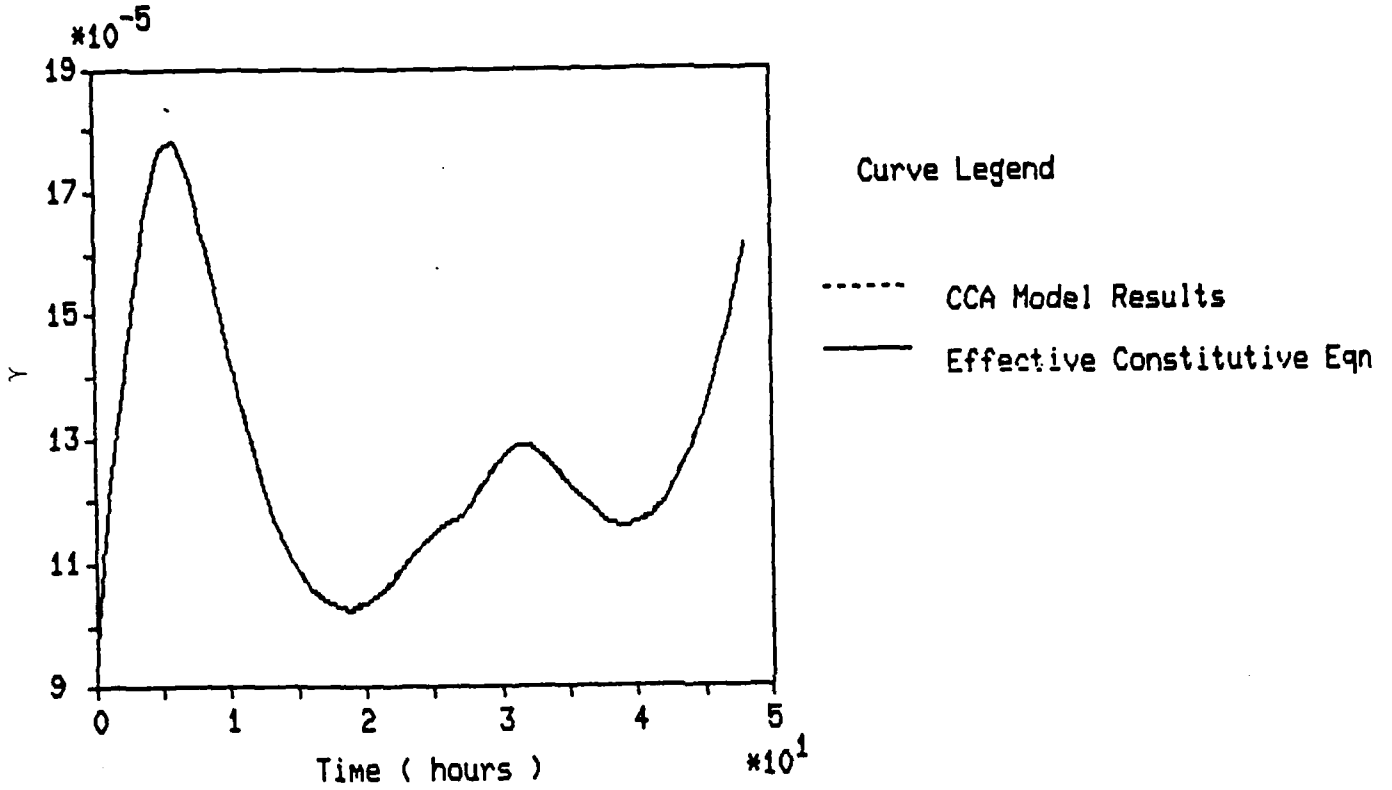

Figure 2.9. Comparison of Axial Shear Strain Results for Simultaneous Axial Shear Stress and Temperature Loads

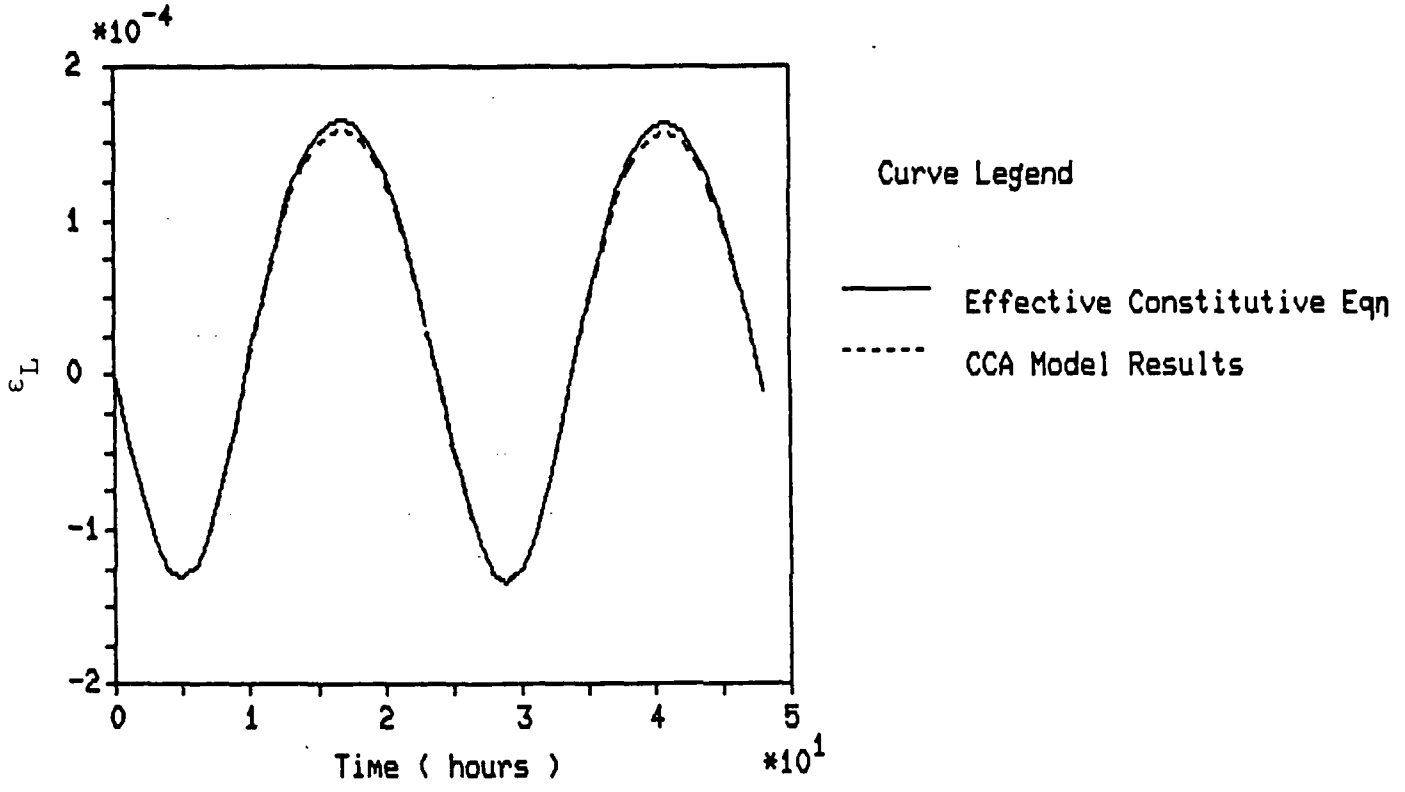

Figure 2.10. Comparison of Thermally Induced Longitudinal Strains

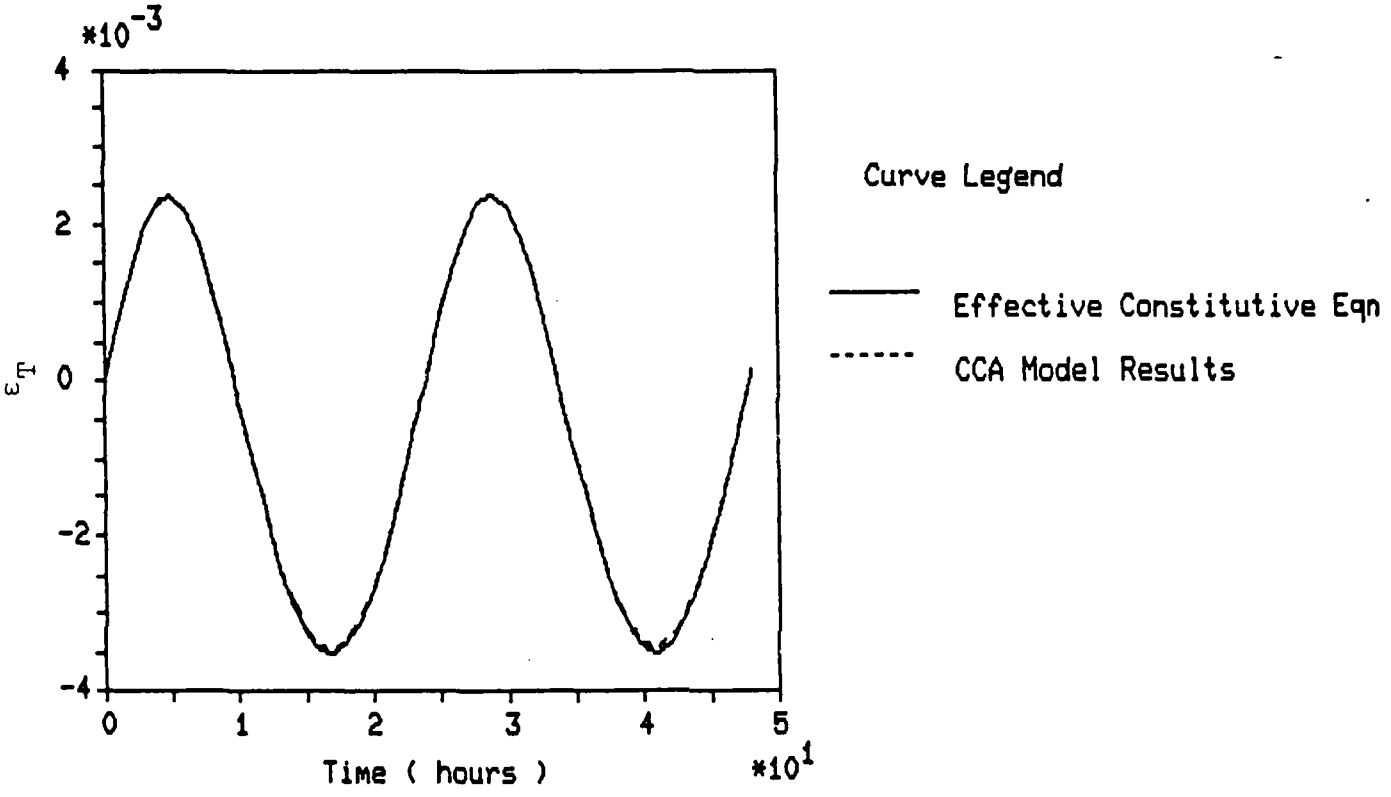

Figure 2.11. Comparison of Thermally Induced Transverse Strains

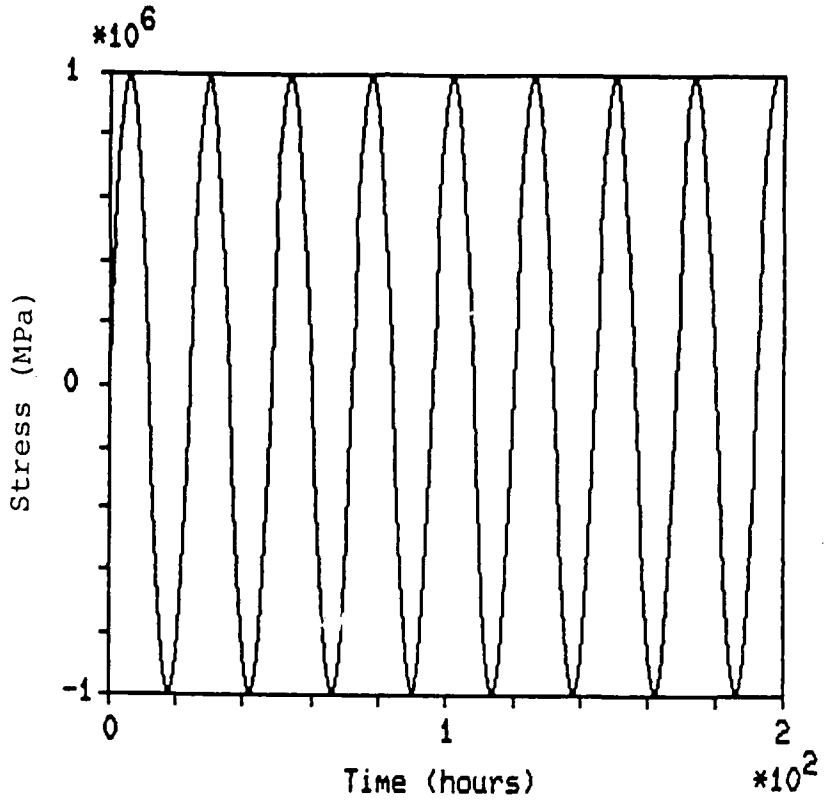

Figure 3.1. Applied Sinusoidal Axial Shear Stress on Unidirectional Carbon/Epoxy Composite Structural Element

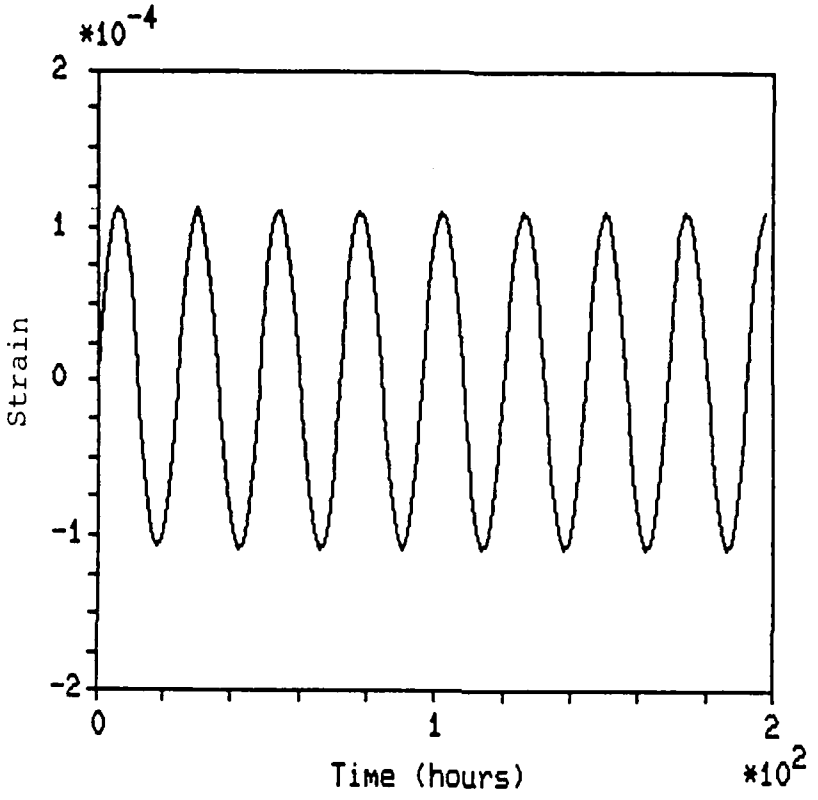

Figure 3.2. Sinusoidal Axial Shear Strain Response for T_σ = 24

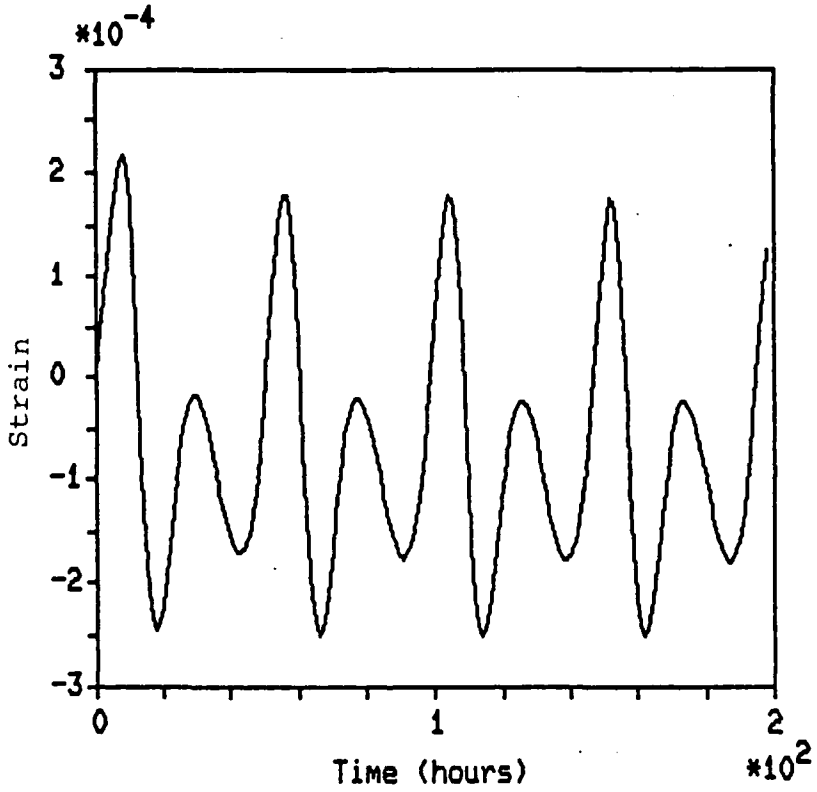

Figure 3.3. Axial Shear Strain for $T_\sigma/T_\phi = 1/2$

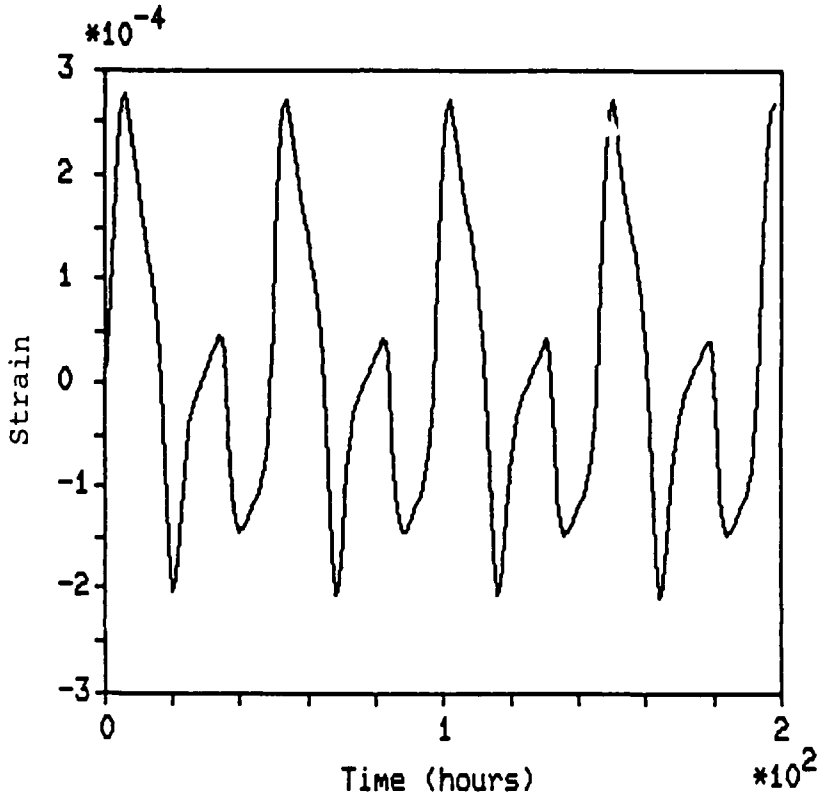

Figure 3.4. Axial Shear Strain for $T_\sigma/T_\phi = 3/2$

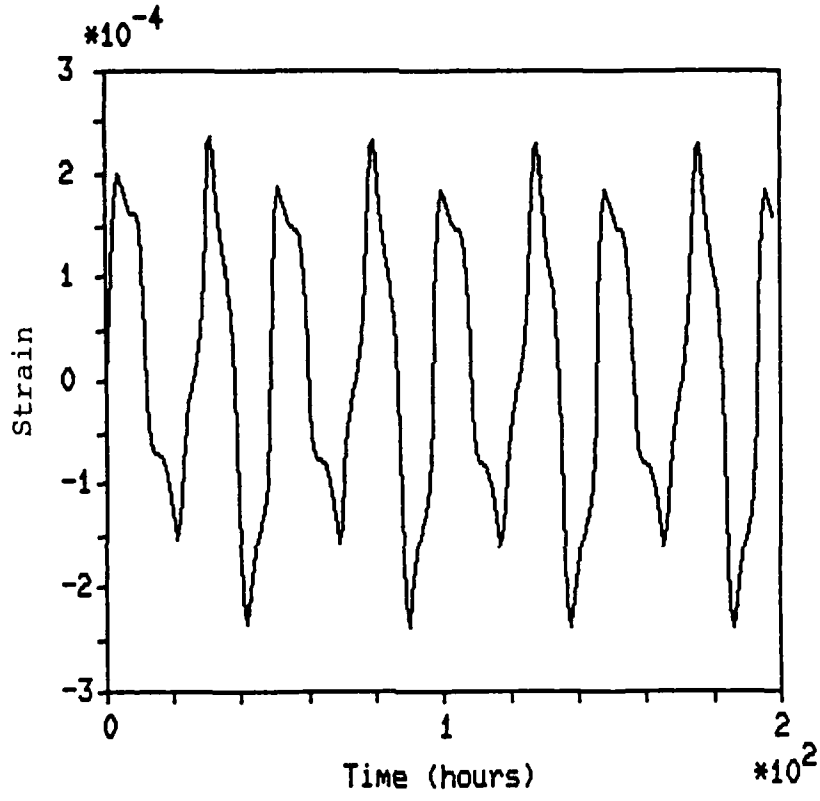

Figure 3.5. Axial Shear Strain for $T_\sigma/T_\phi = 5/2$

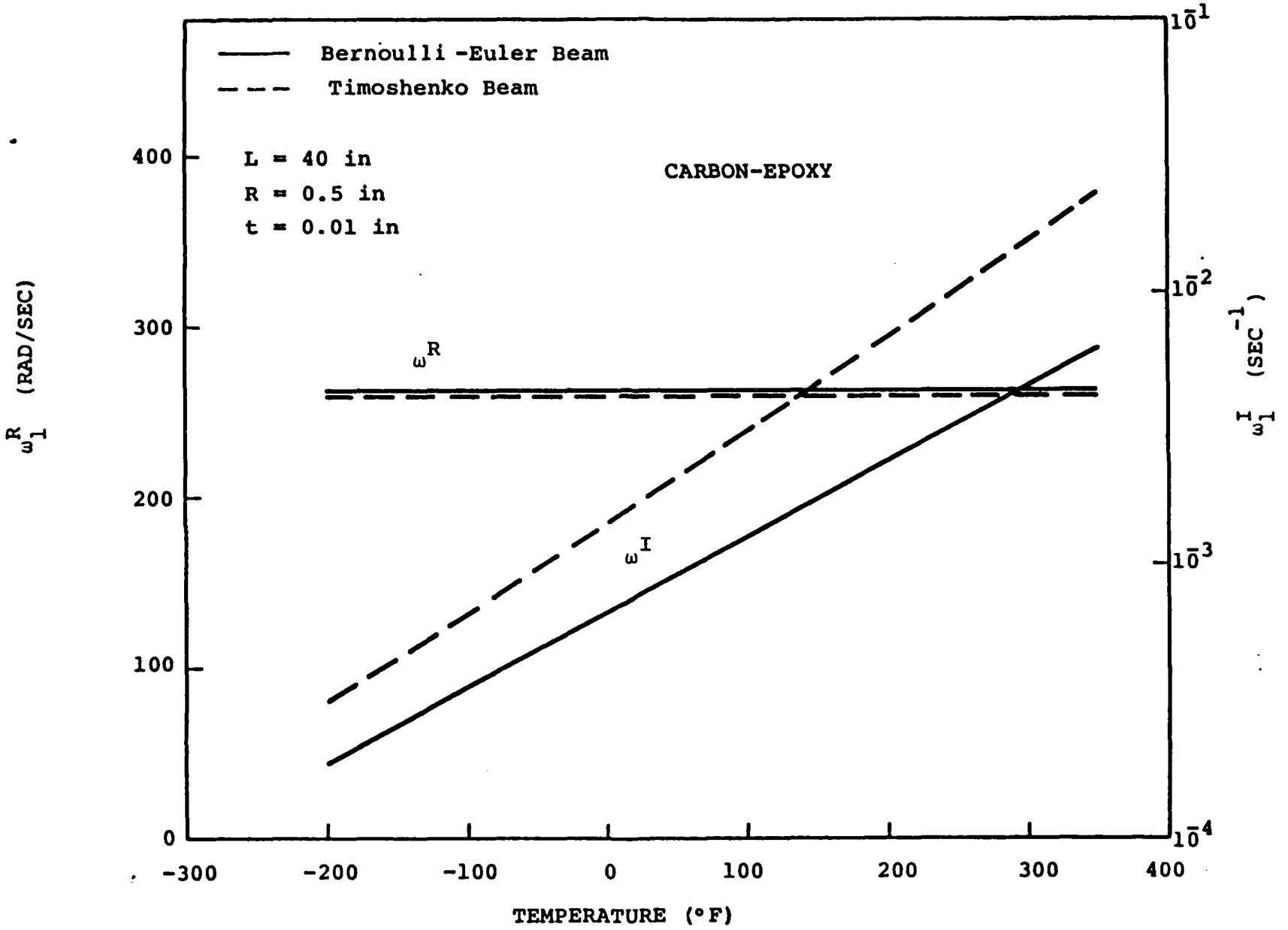

Figure 4.1. Variation of First Mode Natural Frequencies with Temperature for Unidirectional Composite Cantilever Beam

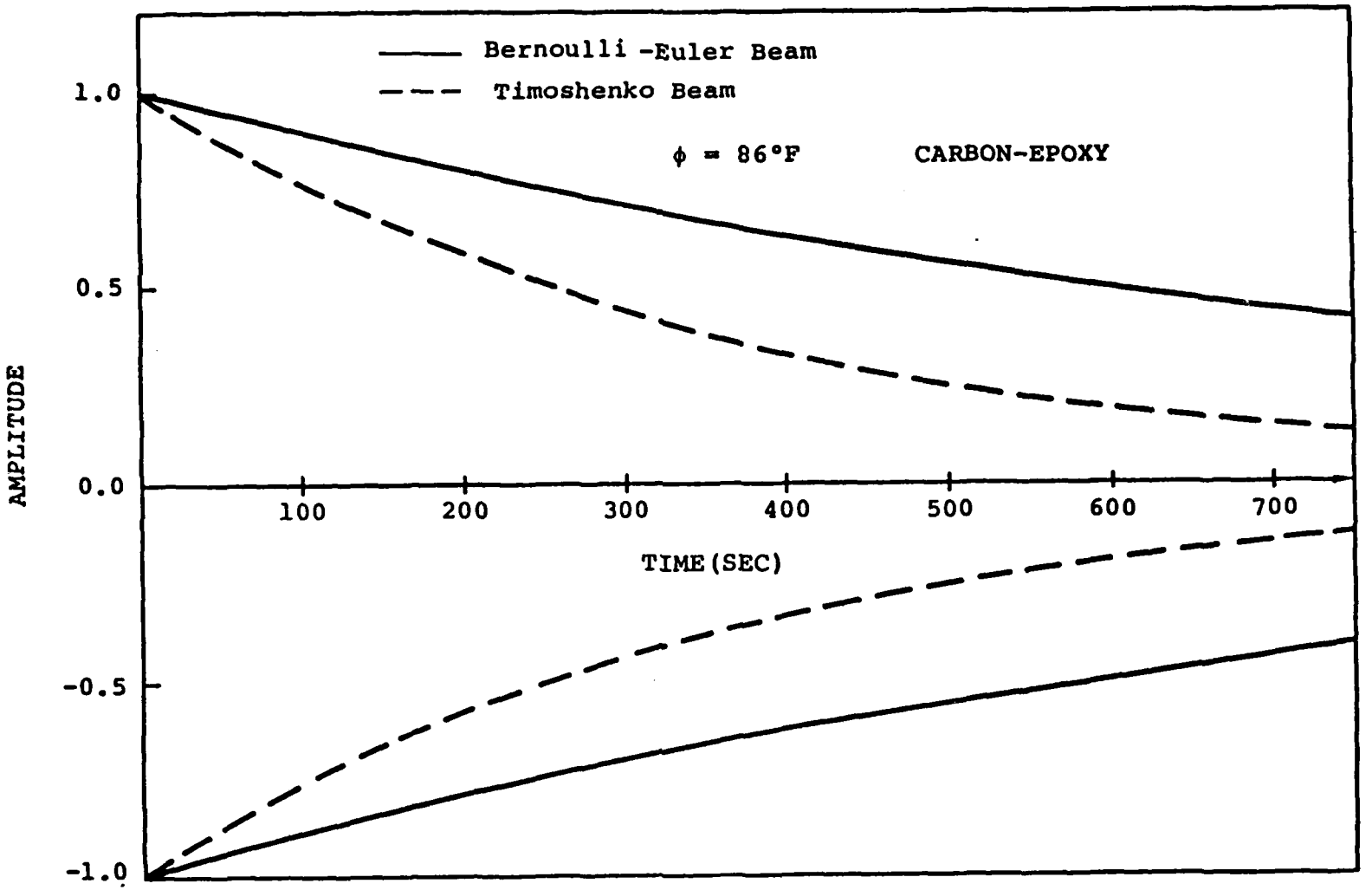

Figure 4.2. Envelope of First Mode Response in Unidirectional Composite Cantilever Beam at Room Temperature

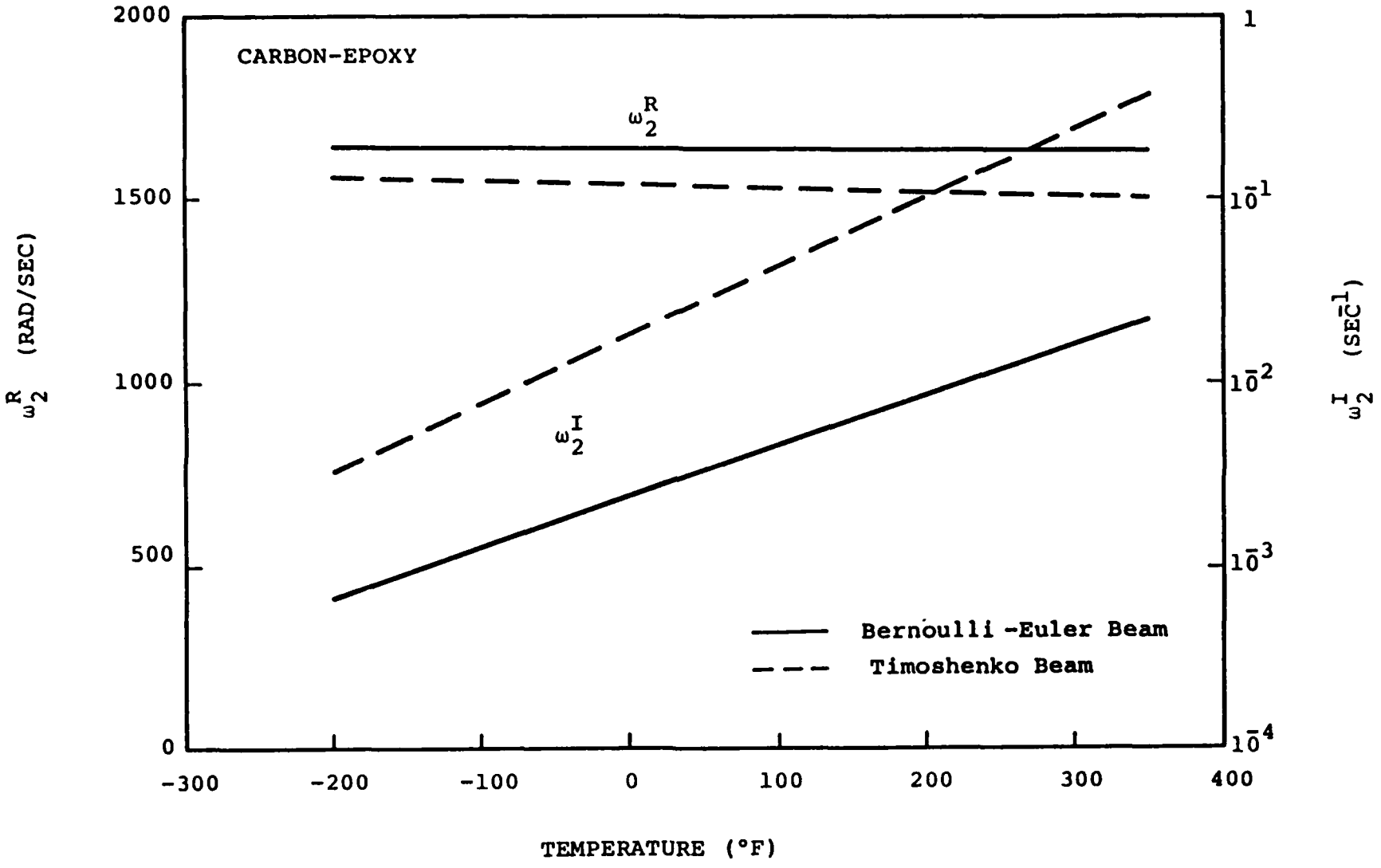

Figure 4.3. Variation of Second Mode Natural Frequencies with Temperature for Unidirectional Composite Cantilever Beam

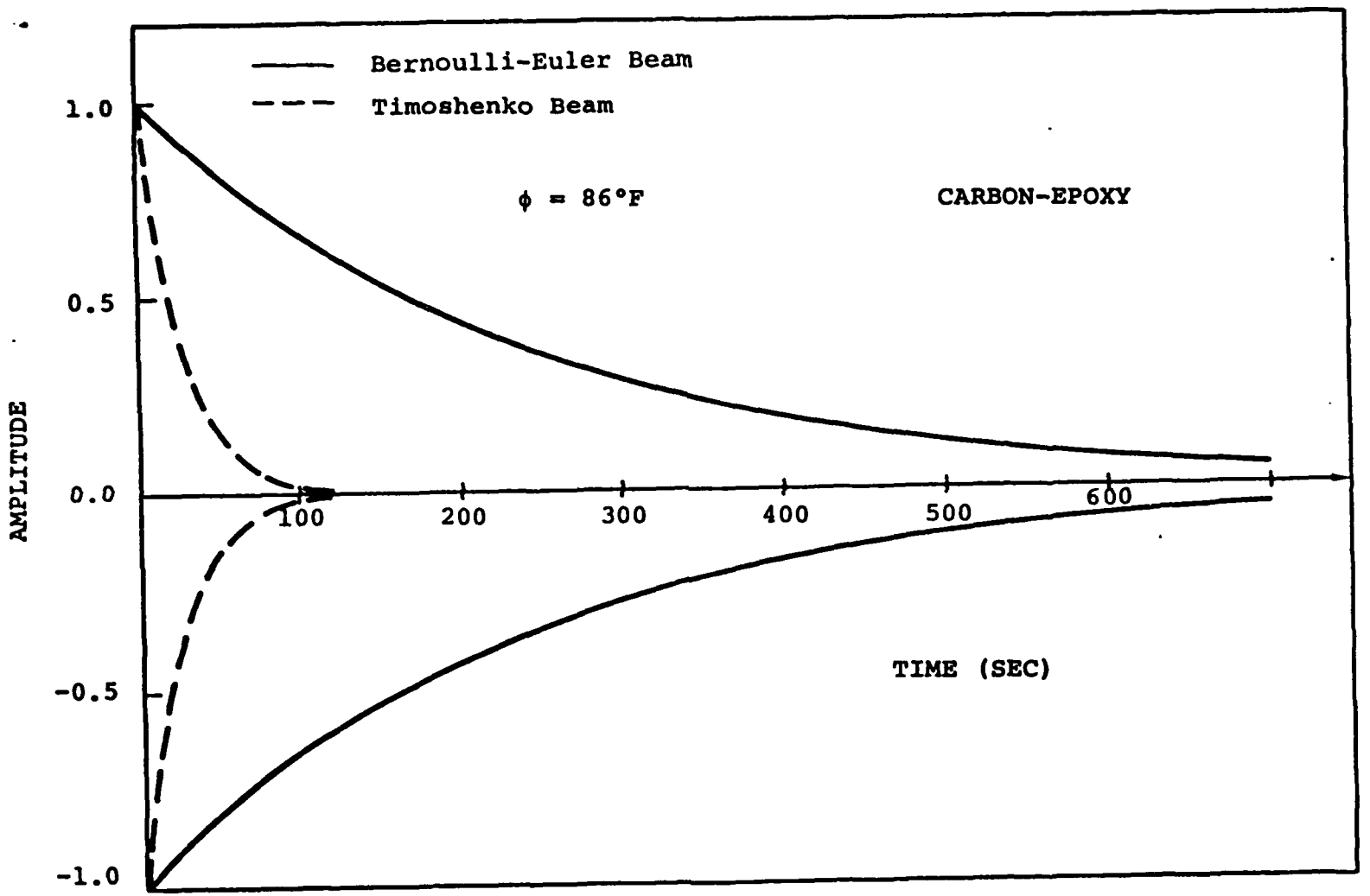

Figure 4.4. Envelope of Second Mode Response in Unidirectional Composite Cantilever Beam at Room Temperature

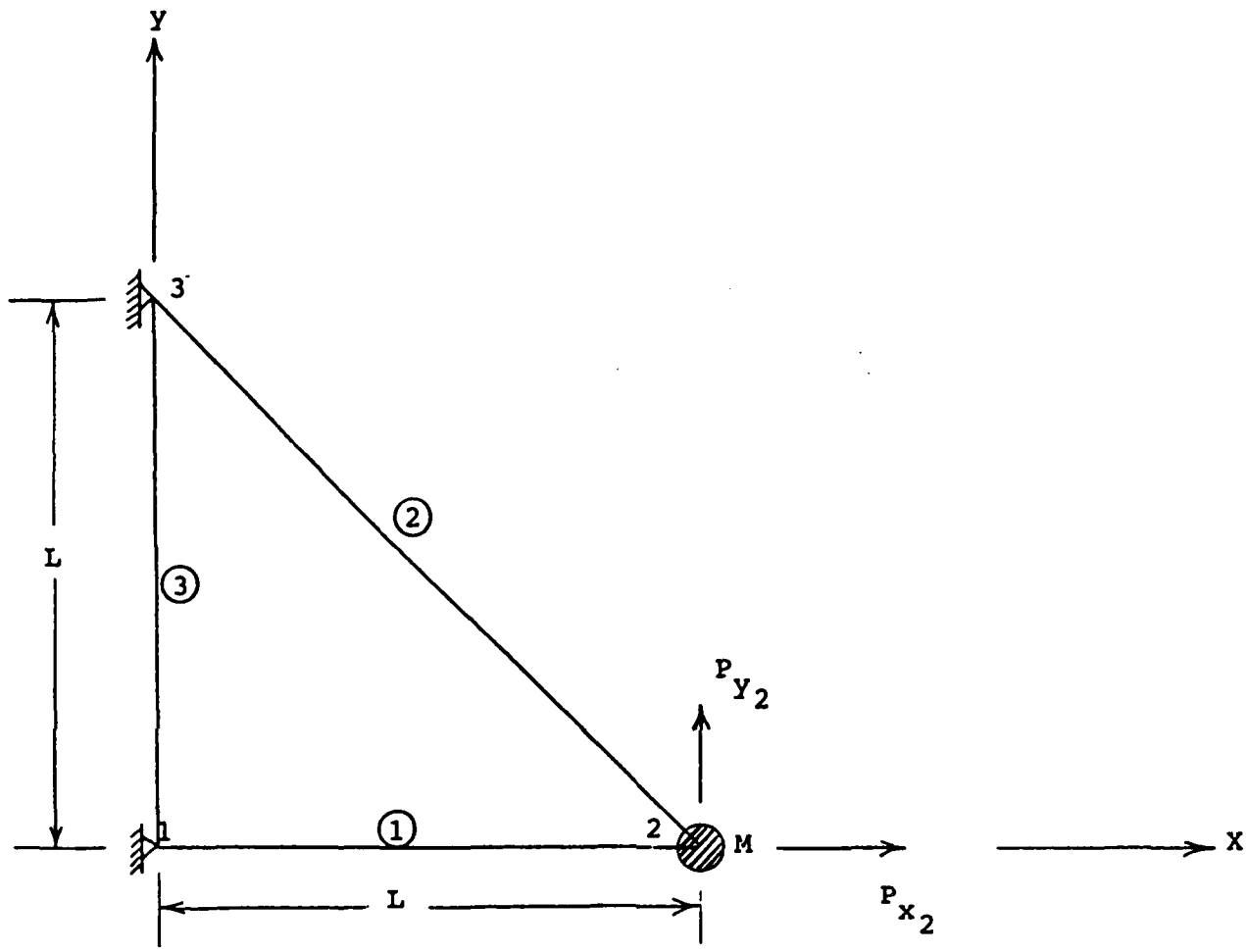

L = 20 m, M = 870 kg, Carbon-Epoxy Truss Members

0° Layup - Fibers Parallel to Axis of Bar

90° Layup - Fibers Perpendicular to Axis of Bar

Figure 4.5. Geometry of Simple Truss Used in Composite Structural Analyses

MODE 1

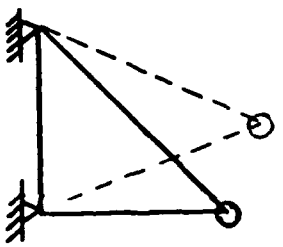

$$\{\phi_1\} = \begin{Bmatrix} .01028 \\ .03234 \end{Bmatrix}$$

MODE 2

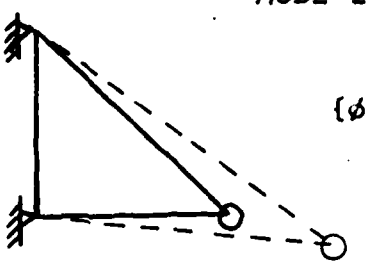

$$\{\phi_2\} = \begin{Bmatrix} 0.03234 \\ -0.01028 \end{Bmatrix}$$

Material Design	f_1 (Hz)	f_2 (Hz)
0° Layup	1.0	2.465
90° Layup	0.208	0.512

Figure 4.6. Eigensolution of Simple Truss with Zero and 90 Degree Layup Composite Members

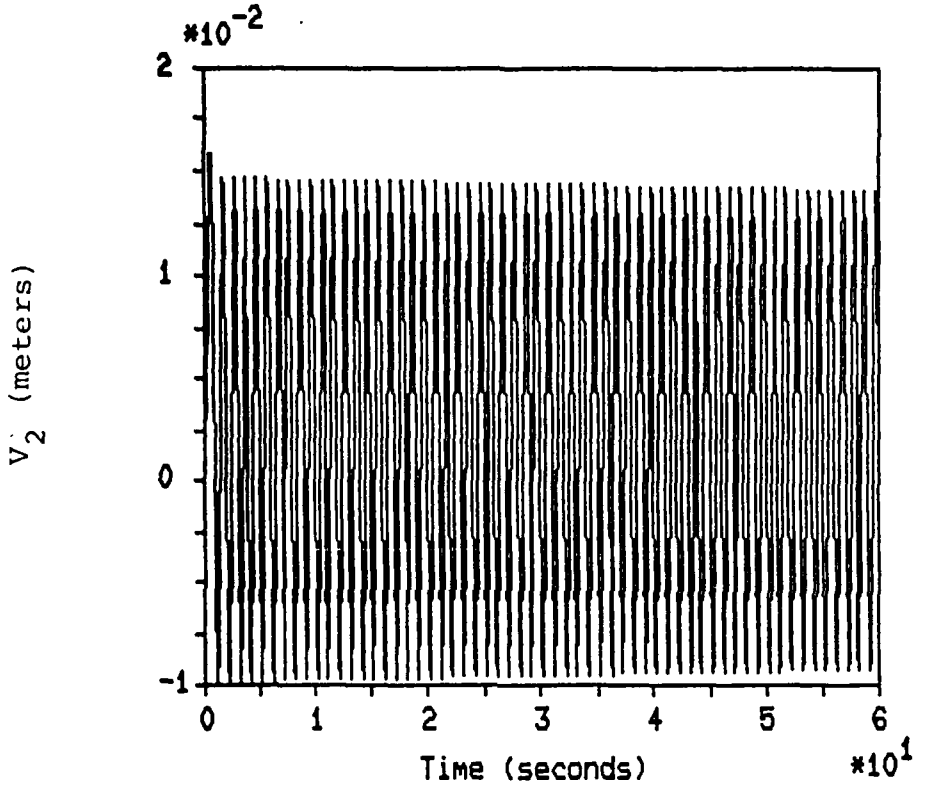

Figure 4.7. Vertical Displacement at Joint 2 Due to Impulsive Horizontal Load at $\Delta\phi$ = 117°K for Truss with Zero Degree Layup Members

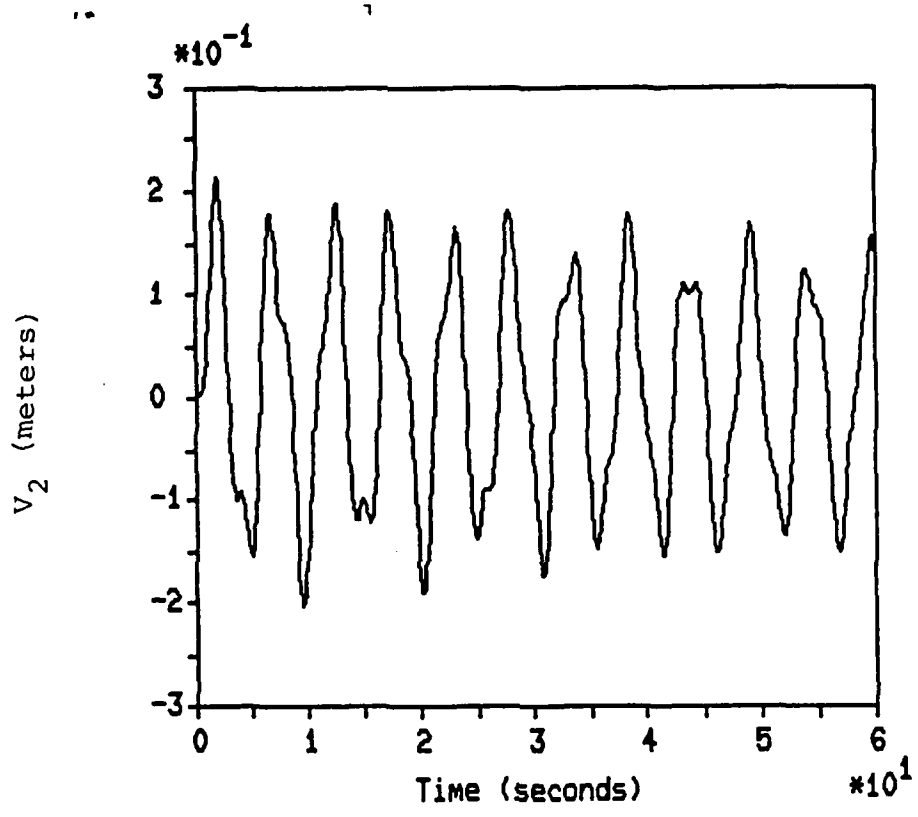

Figure 4.8. Vertical Displacement at Joint 2 Due to Impulsive Horizontal Load at $\Delta\phi$ = 117°K for Truss with 90 Degree Layup Members

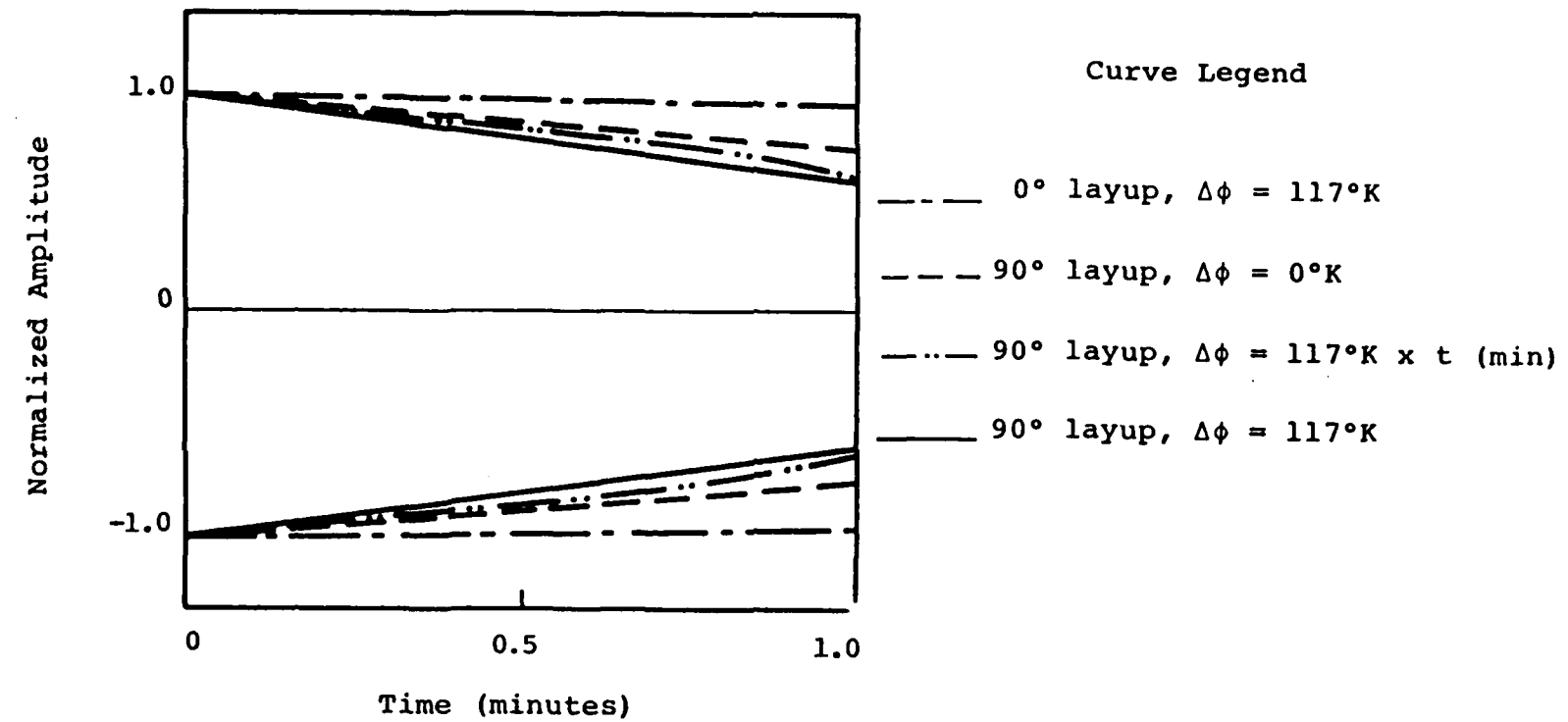

Figure 4.9. Envelopes of Vertical Displacement Response Histories in Truss Due to Impulsive Horizontal Load

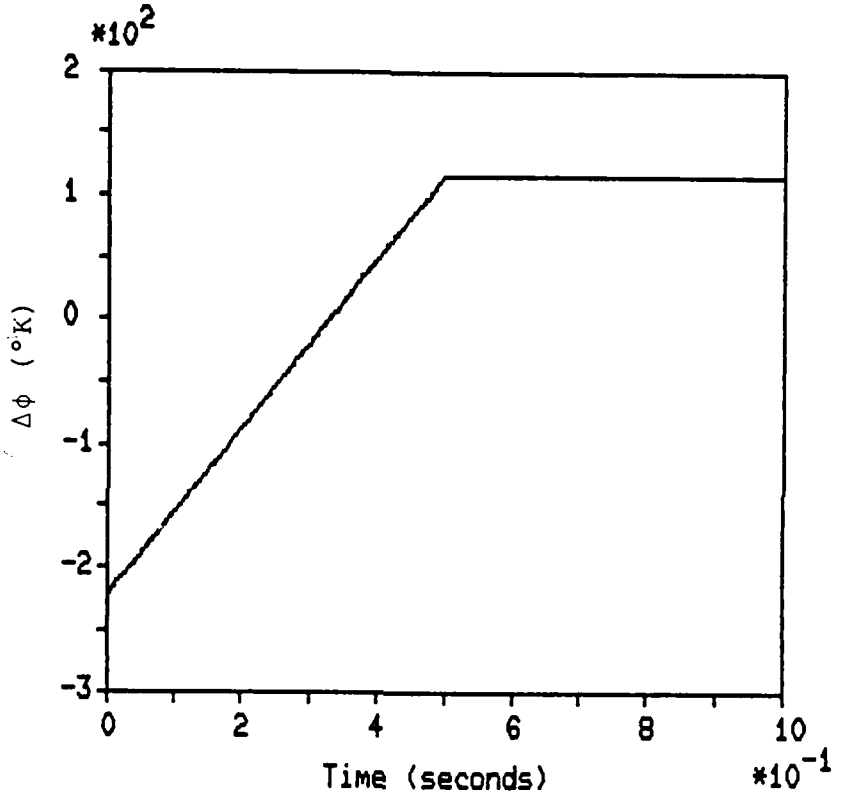

Figure 4.10. Applied Thermal Load on Members of Truss

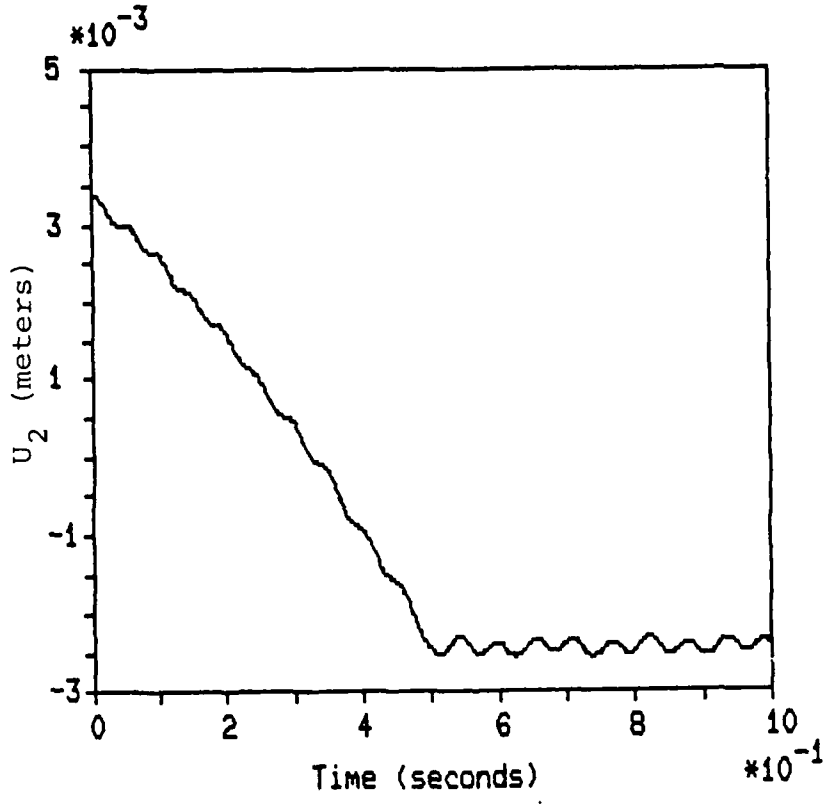

Figure 4.11. Horizontal Displacement History at Joint 2 Due to Thermal Shock Load

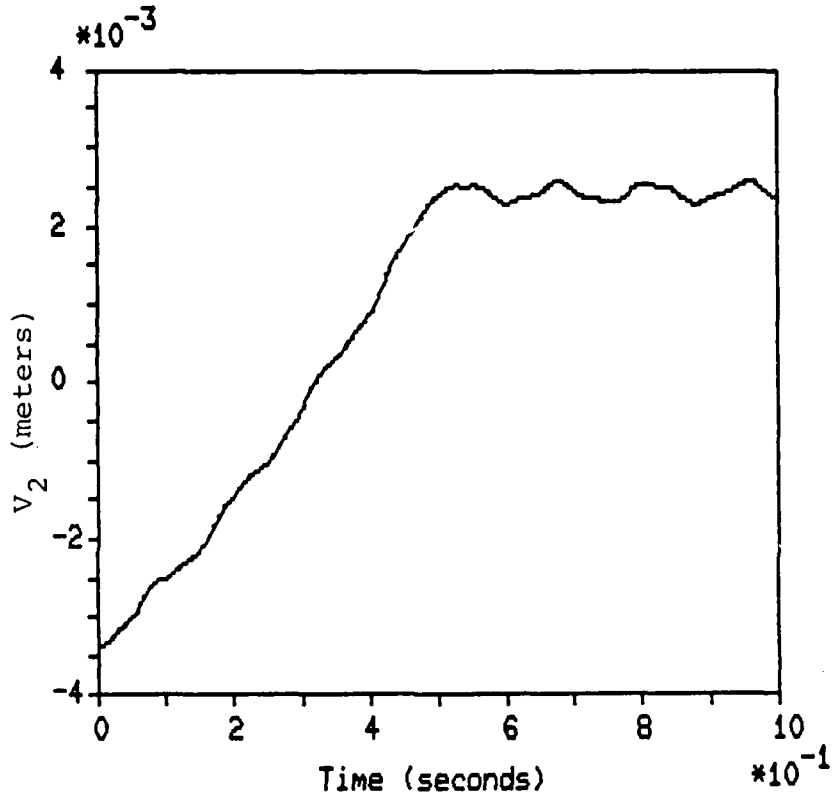

Figure 4.12. Vertical Displacement History at Joint 2 Due to Thermal Shock Load

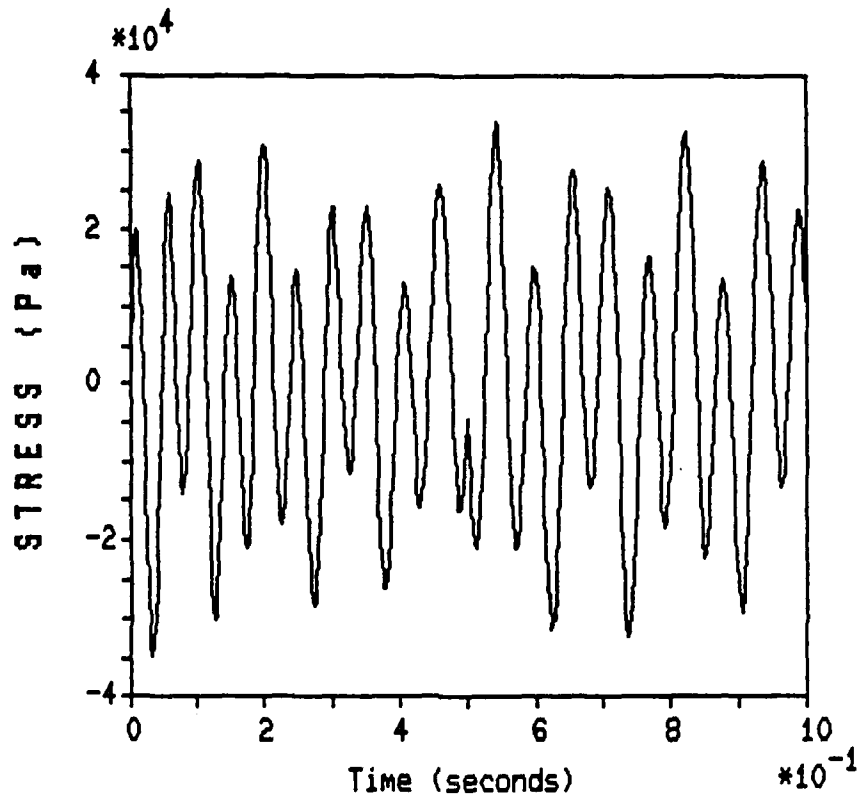

Figure 4.13. Member 1 Stress History for Applied Thermal Shock Load

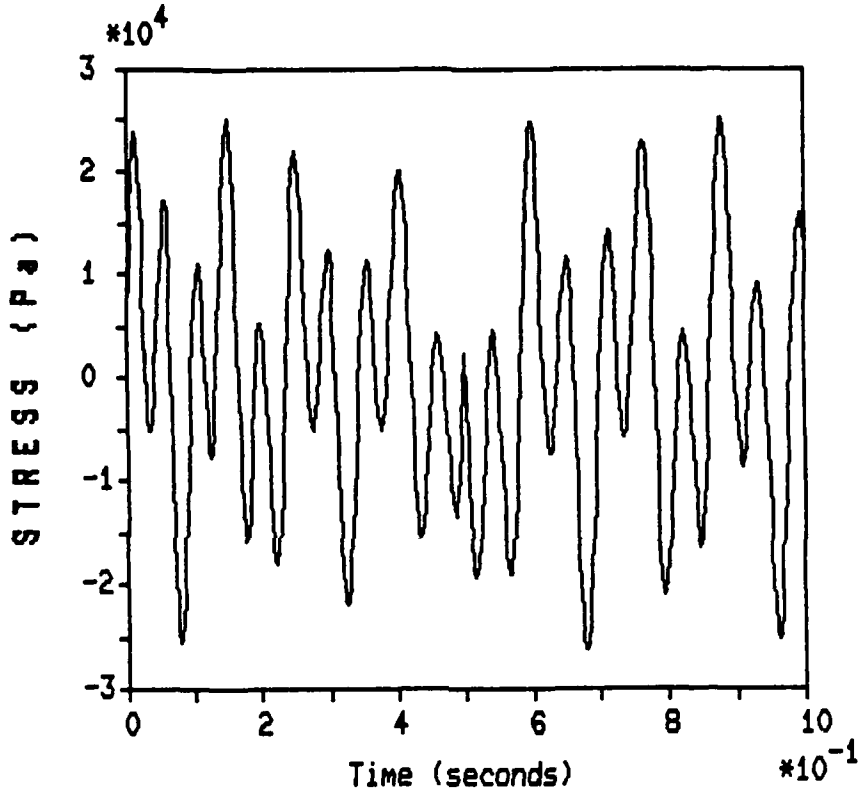

Figure 4.14. Member 2 Stress History for Applied Thermal Shock Load

END

4-87

DTIC